

Fast Radio Bursts: An Extragalactic Enigma

James M. Cordes and Shami Chatterjee

Department of Astronomy and Cornell Center for Astrophysics and Planetary Science, Cornell University, Ithaca, New York 14853, USA; email: jmc33@cornell.edu, sc99@cornell.edu

Annu. Rev. Astron. Astrophys. 2019. 57:417–65

The *Annual Review of Astronomy and Astrophysics* is online at astro.annualreviews.org

<https://doi.org/10.1146/annurev-astro-091918-104501>

Copyright © 2019 by Annual Reviews.
All rights reserved

ANNUAL REVIEWS **CONNECT**

www.annualreviews.org

- Download figures
- Navigate cited references
- Keyword search
- Explore related articles
- Share via email or social media

Keywords

transients, radio surveys, magnetars, neutron stars, extragalactic sources

Abstract

We summarize our understanding of millisecond radio bursts from an extragalactic population of sources. Fast radio bursts (FRBs) occur at an extraordinary rate, thousands per day over the entire sky with radiation energy densities at the source about ten billion times larger than those from Galactic pulsars. We survey FRB phenomenology, source models and host galaxies, coherent radiation models, and the role of plasma propagation effects in burst detection. The FRB field is guaranteed to be exciting: New telescopes will expand the sample from the current \sim 80 unique burst sources (and only a few secure localizations and redshifts) to thousands, with burst localizations that enable host-galaxy redshifts emerging directly from interferometric surveys.

- FRBs are now established as an extragalactic phenomenon.
- Only a few sources are known to repeat. Despite the failure to re-detect other FRBs, they are not inconsistent with all being repeaters.
- FRB sources may be new, exotic kinds of objects or known types in extreme circumstances. Many inventive models exist, ranging from alien spacecraft to cosmic strings, but those concerning compact objects and supermassive black holes have gained the most attention. A rapidly rotating magnetar is a promising explanation for FRB 121102 along with the persistent source associated with it, but alternative source models are not ruled out for it or other FRBs.
- FRBs are powerful tracers of circumsource environments, “missing baryons” in the intergalactic medium (IGM), and dark matter.
- The relative contributions of host galaxies and the IGM to propagation effects have yet to be disentangled, so dispersion measure distances have large uncertainties.

Contents

1. INTRODUCTION	418
2. SUMMARY OF THE FRB PHENOMENON	422
2.1. Numbers and Rates	422
2.2. Follow-Up Observations: Trials and Tribulations	425
2.3. Dispersion and Scattering of FRBs	426
2.4. Time-Frequency Burst Structure	428
2.5. Polarization	428
2.6. Localizations	429
2.7. Energetics	430
2.8. Are Bursts From Rotation or Temporal Modulation?	430
2.9. Fast Transients, Brightness Temperatures, and Coherent Radiation	431
3. THE ASTRO-OPTICS OF FRBs	432
3.1. Galactic Propagation	432
3.2. Propagation Model for Bursts	433
3.3. Scattering in Host Galaxies, Intervening Galaxies, and the Intergalactic Medium	433
3.4. Propagation Factors that Affect FRB Detections	434
4. THE REPEATING FRB 121102	438
4.1. The Persistent Radio Counterpart Associated with FRB 121102	441
4.2. Burst Periodicity and Sporadicity	442
4.3. Scattering of FRB 121102	442
4.4. Constraints on the Magnetohydrodynamic Circumsource Medium	443
5. HOST GALAXIES AND COUNTERPARTS	443
6. SURVEYS AND POPULATIONS	444
6.1. The Fluence–DM Distribution	444
6.2. Some Population Numbers	446
6.3. Modulated Luminosity Functions and Detection Numbers	446
7. THE FRB DISTANCE SCALE	448
7.1. Deconstructing Dispersion Measure	449
7.2. Dispersion Measure–Redshift Relation	449
7.3. The τ –Dispersion Measure Relation	451
8. SOURCES, RADIATION PROCESSES, AND CENTRAL ENGINES	453
8.1. Radiation Processes and Beaming	453
8.2. Source Models	455
8.3. Demographics	456
8.4. Young, Rapidly Rotating Neutron Stars	457
8.5. AGNs Interacting with Neutron Stars	459
9. FRBs AS TOOLS FOR ASTROPHYSICS AND FUNDAMENTAL PHYSICS	459
10. PROSPECTS FOR FUTURE WORK	460

1. INTRODUCTION

Fast radio bursts (FRBs) are millisecond-duration pulses that originate from as-yet-unidentified extragalactic sources. They are similar in some respects to pulses from Galactic radio pulsars, but the flux density is of order ten billion times larger and their spectra are radically different from

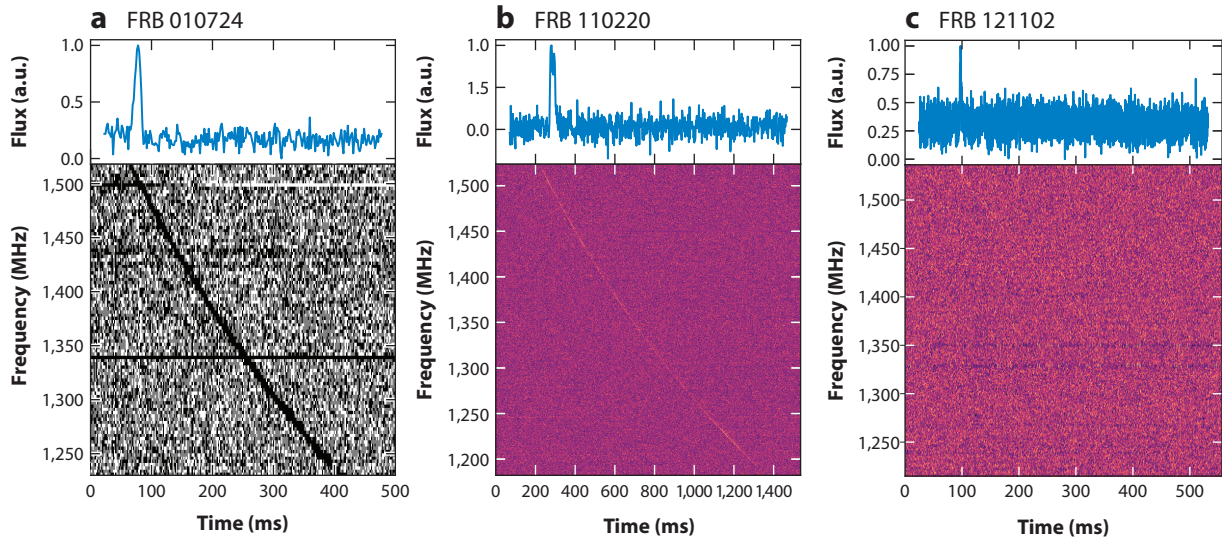


Figure 1

FRB dynamic spectra. In each case, the lower panel shows the sweep of the burst across the time–frequency plane, and the upper panel shows the total pulse intensity after removing the best-fit quadratic dispersion sweep and frequency-averaging across the band. Time and frequency resolutions vary, depending on the instrument. (a) FRB 010724, the first-reported fast radio burst with $\text{DM} = 375 \text{ pc cm}^{-3}$. (b) FRB 110220, detected at Parkes with $\text{DM} = 944.4 \text{ pc cm}^{-3}$, leading to the realization that FRBs were most likely astrophysical in nature. (c) The original detection of FRB 121102 at Arecibo, the first reported non-Parkes FRB, with $\text{DM} = 557.4 \text{ pc cm}^{-3}$. Panels use data taken with permission from (a) Lorimer et al. (2007), (b) Thornton et al. (2013), and (c) Spitler et al. (2014). Abbreviations: DM, dispersion measure; FRB, fast radio burst.

most pulsar spectra and most other radio sources. To date¹ bursts from over 80 distinct sources have been reported in the literature since the discovery of the first FRB (Lorimer et al. 2007). Of these, multiple bursts have been detected from only a few FRB sources and only a few have secure localizations. FRB 121102, the first to be localized, is in a star-forming region in a dwarf galaxy with a luminosity distance of about 1 Gpc.

The nature of FRBs and their sources are thus first and foremost a bona fide mystery about which we have several important clues that will likely lead soon to an understanding of the phenomenon. In addition, FRBs are also superb tools for probing the diverse media with dramatically different conditions along their lines of sight, including the immediate source environment, their host galaxies, and the cosmic web.

Short duration pulses have been known in radio astronomy since the discovery of pulsars in 1967. Recognition that their radio-frequency (ν)-dependent arrival times followed the characteristic $\text{DM} \nu^{-2}$ scaling law expected for a tenuous, cold plasma was central to establishing an early distance scale for the first pulsars, and the same approach has been taken for FRBs. Here, $\text{DM} = \int_0^d ds n_e$ is the dispersion measure, the integral of the electron density to a source at distance d . Values for Galactic pulsars range from ~ 1 to $1,700 \text{ pc cm}^{-3}$, where the units follow from distances expressed in parsecs and electron densities in cm^{-3} . Figure 1 shows FRB dynamic spectra where the dispersion delays have been retained, whereas subsequent figures (Figures 2 and 3) show them with the delay removed.

¹Up to February 1, 2019. Literature review covered up to December 1, 2018, except for early results from CHIME (Canadian Hydrogen Intensity Mapping Experiment).

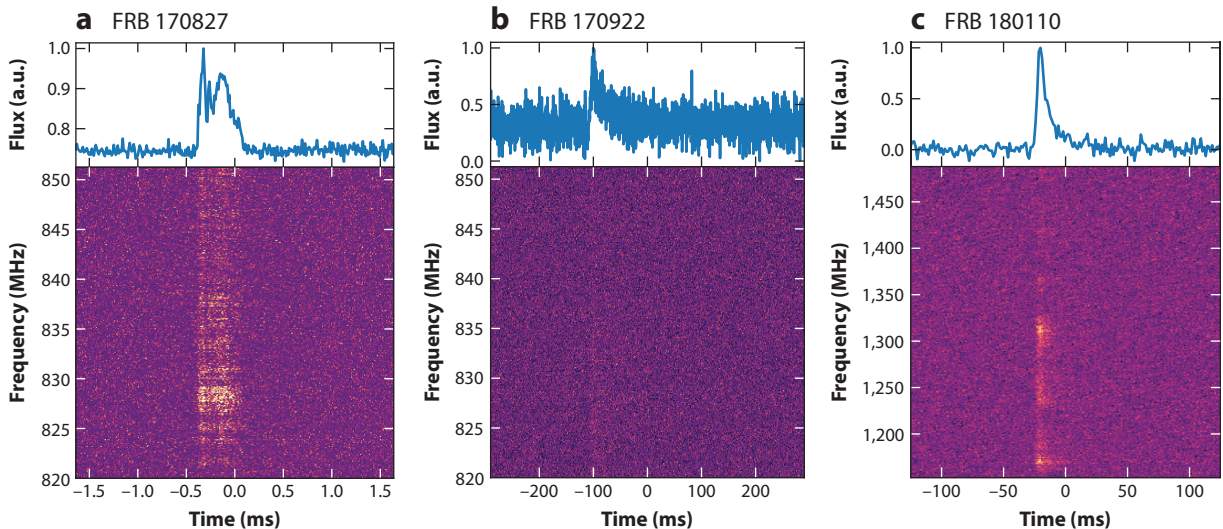


Figure 2

FRB dynamic spectra. In each case, the lower panel shows the burst on the time–frequency plane after removing the best-fit quadratic pulse dispersion sweep, and the upper panel shows the dedispersed pulse total intensity after frequency-averaging across the band. Time and frequency resolutions vary, depending on the instrument. (a) FRB 170827, detected at UTMOST with $\text{DM} = 899 \text{ pc cm}^{-3}$. Voltage capture was triggered after real-time detection, and coherent dedispersion reveals fine structure in the burst. (b) FRB 170922, detected at UTMOST with $\text{DM} = 1,111 \text{ pc cm}^{-3}$ and with very significant pulse scattering. (c) FRB 180110, a bright burst detected with ASKAP in fly’s-eye mode with $\text{DM} = 716 \text{ pc cm}^{-3}$. Panels use data taken with permission from (a) Farah et al. (2018), (b) Farah et al. (2017), and (c) Shannon et al. (2018). Abbreviations: ASKAP, Australian Square Kilometre Array Pathfinder; DM, dispersion measure; FRB, fast radio burst; UTMOST, the updated Molonglo Observatory Synthesis Telescope.

The first FRB (Lorimer et al. 2007) showed dispersive arrival times combined with broadening by multipath scattering from small-scale fluctuations in electron density. The too-large-to-be-Galactic value of DM led to the conjecture that the source was extragalactic. FRBs viewed at high Galactic latitudes b receive Galactic contributions of about $30 \text{ pc cm}^{-3} / \sin |b|$ compared to $\text{DM} \sim 375 \text{ pc cm}^{-3}$ for the Lorimer burst (FRB 010724). However, establishing FRBs as an astrophysical phenomenon took another six years with the identification of further examples (Thornton et al. 2013), albeit from the same Parkes telescope in Australia. The discovery of a burst using the Arecibo radio telescope (Spitler et al. 2014) gave further credence to the phenomenon.

The slow acceptance of FRBs as an extragalactic phenomenon is a consequence of a rather long history of false positives, the fact that some Galactic objects, including pulsars, show a high degree of intermittency, and the idea that unmodeled HII regions (Kulkarni et al. 2014) or stars (Maoz et al. 2015) in the Milky Way (MW) might be responsible for the large measured values of DM. And, of course, radio-frequency interference (RFI) from artificial terrestrial sources can mimic dispersed pulses (Petroff et al. 2015c).

Some Galactic pulsars are sufficiently intermittent that they were discovered as single-pulse emitters and only subsequently determined to be periodic with properties otherwise identical to pulsars. They were consequently described as rotating radio transients (RRATs; McLaughlin et al. 2006). A handful of RRATs, like most FRBs, have defied redetection. However, their DM values are consistent with residence in the MW, so—as the jargon currently stands—they are not FRBs. Eventually, a Galactic FRB may be identified as a very bright event that saturates radio receivers in telescopes and in telephones.

In the early days of pulsar astronomy, attempts were made to detect dispersed radio pulses from high-energy objects, such as the X-ray sources Sco X-1 and Cyg X-1 (Taylor et al. 1972).

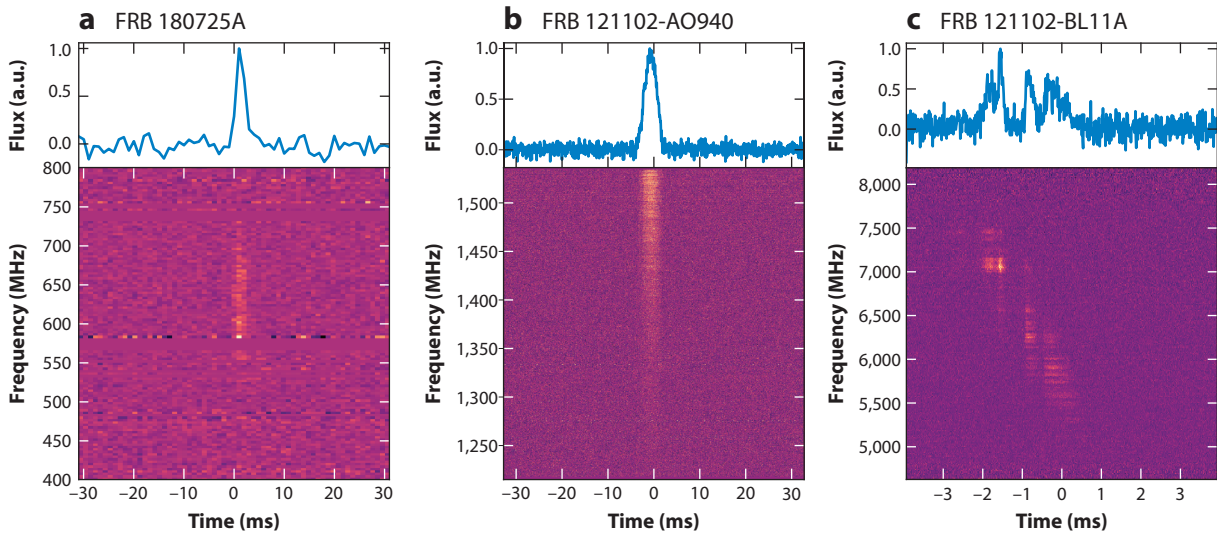


Figure 3

FRB dynamic spectra. As in **Figure 2**, the lower panel shows the burst on the time–frequency plane after removing the best-fit quadratic pulse dispersion sweep, and the upper panel shows the dedispersed pulse total intensity after frequency-averaging across the band. Time and frequency resolutions vary, depending on the instrument. (a) FRB 180725A, the first FRB detected at CHIME and at frequencies down to 550 MHz with $\text{DM} = 716.6 \text{ pc cm}^{-3}$. (b) One of the first and brightest redetections of FRB 121102 at Arecibo at 1.2–1.6 GHz. (c) Another detection of FRB 121102 at the Green Bank Telescope but at 4–8 GHz. Precise localization enabled high-frequency observations, and the known DM allowed coherent dedispersion, revealing extensive pulse structure at these higher frequencies. Panels use data taken with permission from (a) CHIME/FRB Collab. et al. (2019a), (b) Spitler et al. (2016), and (c) Gajjar et al. (2018). Abbreviations: CHIME, Canadian Hydrogen Intensity Mapping Experiment; DM, dispersion measure; FRB, fast radio burst.

None were found, and it is now understood that strong coherent radio emission does not occur in accreting X-ray sources. Later, Linscott & Erkes (1980) used a fast (submillisecond) spectrometer at Arecibo to search for bursts from the blazar M87. In this case, dispersed pulses were claimed but not confirmed by others, and therefore they were dismissed as RFI or artifacts of the hardware. In retrospect, given the apparent nonrepeatability of most FRBs, one wonders whether the M87 pulses were in fact real and await confirmation!

Other attempts were made at low frequencies, including work using the Molonglo Observatory Synthesis Telescope (MOST) by Amy et al. (1989) at 0.84 GHz that detected many pulsars in $\sim 4,000$ h along with considerable RFI and unclassified events in the \sim millisecond range that were not obviously due to RFI. On average per 12 h observation, about one such unclassified event occurred that was “not ruled out as being of celestial origin” (Amy et al. 1989, p. 173). The threshold for this survey was ~ 15 – 50 Jy ms for widths from 1 to 10 ms. A two-station survey at 0.27 GHz (Huguenin & Moore 1974) was motivated by predictions that SNe would emit narrow $\lesssim 1$ -s pulses. The system had ~ 1 sr field of view and relied on pulse dispersion to discriminate RFI from events of celestial origin. Unfortunately, none were found at levels above $\sim 10^4$ Jy for widths from 20 ms to 1 s. The notion that evaporating black holes (BHs) would emit narrow radio bursts (Rees 1977) motivated several detection attempts (e.g., O’Sullivan et al. 1978) and has been referred to as a possible source class for FRBs. However, the original idea involved physics that is no longer thought applicable (M. Rees, private communication).

An early example of multimessenger astronomy involved searches for radio pulses that coincided with gravitational wave (GW) bursts from the Galactic center (GC; Hughes & Retallack 1973, Edwards et al. 1974, and references therein) claimed by Weber (1970). Dispersion delays

between GW and radio bursts were considered in the analyses but the time resolutions were long (1 and 10 s, respectively). No GW-radio coincidences were found but astrophysical radio events were claimed to contribute to the overall results obtained by Hughes & Retallack (1973).

The role of dispersion delays between any prompt radio emission from gamma-ray bursts (GRBs; Palmer 1993) was built into response time goals and detection criteria for low-frequency observations triggered by GRB detections (e.g., Baird et al. 1975, Dessenne et al. 1996). Similar considerations about dispersion effects enter into multiwavelength/messenger studies of FRBs.

This incomplete but representative historical summary illustrates that the techniques used today for FRB studies have their precedents in long-ago experiments, albeit now with much greater sensitivity and insights into the properties of transient radio emission.

The timing of this review is at an inflection point when FRBs have been well established as an extragalactic phenomenon, but there is not yet a deep understanding of the underlying astrophysics nor their population statistics. This will change with the rise of high duty cycle, wide-field surveys that are just beginning to dramatically increase the discovery rate. The review necessarily excludes insights that will emerge from these surveys and their multiwavelength follow-up. However, topics in fundamental astrophysics, methods, and interpretation that we discuss will hopefully have sustained relevance.

In this review, we summarize what is currently known about the FRB phenomena, the source physics that may underlie them, and their potential as tools for extragalactic astrophysics and extreme physics. The following questions motivate the content and organization of this review: Do all FRB sources repeat? What is the FRB distance scale? Do all FRBs originate from the same type of object? What can FRBs be used for? And finally, Where will the FRB field be in the long term (10 years)?

2. SUMMARY OF THE FRB PHENOMENON

FRBs are found using data that are essentially the same as those used in pulsar surveys, namely high time resolution spectra ($\sim 100 \mu\text{s}$) with $\sim 1,000$ frequency channels across a total bandwidth of hundreds of megahertz. The key difference is that pulsar surveys seek periodic signals using Fourier methods, which become insensitive to periods that are not small compared to data spans and, of course, are completely insensitive to single pulses. Although individual giant pulses (GPs) from pulsars have long been a known phenomenon, from the mid-1970s on, researchers were largely focused on finding relativistic binary pulsars for tests of General Relativity and millisecond pulsars for use in pulsar timing arrays to detect nanohertz gravitational waves (with exceptions of course). Giant pulses from the Crab pulsar and a few other objects were well studied during this period (and to the present) but were considered a niche subject with ties to high-energy emission.

Attitudes changed during the 1990s because of interests in finding radio counterparts to GRBs and recognition that the discovery phase space for fast transients was essentially unexplored territory. Discoveries of RRATs and FRBs followed directly from the decision to search for single pulses in pulsar survey data. In other words, FRBs were discovered because of attitude adjustment, not from technological innovation. However, follow-up observations of FRBs (especially localizations) have required innovations.

2.1. Numbers and Rates

To date, FRBs have been detected from over 80 distinct sources in a variety of surveys (**Table 1**) since the original event from 2001 was reported in 2007.² Until recently, most FRBs were

²As of February 1, 2019; the Fast Radio Burst Catalog (FRBCAT) is available at <http://www.frbcat.org> (Petroff et al. 2016).

Table 1 Large-scale surveys at 1.4 GHz that constrain FRB population estimates

Telescope/Survey	\mathcal{F}_{\min} (Jy ms)	$\Omega_s T$ (deg 2 h)	N_{frb}	$\Gamma_{\text{frb}}^{\text{a}}$ (sky $^{-1}$ day $^{-1}$)	References
Parkes/all^b	2	4,400	19	$1.7^{+1.5}_{-0.9} \times 10^3$	Bhandari et al. (2018)
Parkes/HTRU(h)	2	1,549	9	$2.5^{+3.2}_{-1.6} \times 10^3$	Thornton et al. (2013), Champion et al. (2016)
Parkes/HTRU(m)	2	694	0	$\lesssim 1.4 \times 10^3$	Petroff et al. (2014)
Parkes/SUPERB	2	1,621	5	$1.7^{+1.5}_{-0.9} \times 10^3$	Bhandari et al. (2018), Keane et al. (2018)
Arecibo/PALFA^c					
Outer Galaxy					Spitler et al. (2014)
Main beam	0.065	6.2	1	$1.6^{+6}_{-1.5} \times 10^5$	FRB 121102
Sidelobes	0.350	29.7	1	$3.1^{+12}_{-3.1} \times 10^4$	FRB 121102
Outer+inner Galaxy					Scholz et al. (2016)
Main beam	0.057	19.5	1	$5.1^{+17.8}_{-4.8} \times 10^4$	FRB 121102
Sidelobes	0.300	93	1	$1.1^{+3.7}_{-1.0} \times 10^4$	FRB 121102
Outer+inner Galaxy					Patel et al. (2018)
Main beam	0.044	12.7	1	$7.8^{+25.6}_{-7.6} \times 10^4$	FRB 141113
Sidelobes	0.239	60	1	$1.6^{+7.5}_{-1.6} \times 10^4$	FRB 141113
ASKAP/Fly's Eye	29.2	5.1×10^5	20	37 ± 8	Shannon et al. (2018)

^aThe mean FRB rate is $4\pi \times (180/\pi)^2 \times 24 \times N_{\text{frb}}/\Omega_s T$, but the rates given account for fluence completeness (Keane & Petroff 2015).

^bThis line includes all Parkes observations reported by Bhandari et al. (2018), their table 5, which includes their FRB detections as well as 14 from the HTRU and SUPERB surveys.

^cArecibo values are for the subsurveys yielding FRB 121102 (Spitler et al. 2014, Scholz et al. 2016) or FRB 141113 (Patel et al. 2018). The analyses consider detection in the main lobes of the 7-beam ALFA receiver or in the sidelobes, which have a larger solid angle at lower sensitivity. The Spitler et al. analysis considers only the subsurvey of the outer Galaxy, whereas the other analyses consider the inner and outer Galaxy subsurveys together.

Abbreviations: ASKAP, Australian Square Kilometre Array Pathfinder; HTRU, High Time Resolution Universe; PALFA, pulsar survey using ALFA (Arecibo L-Band Feed Array); SUPERB, Survey for Pulsars and Extragalactic Radio Bursts.

discovered predominantly at ~ 1.5 GHz, initially with the Parkes telescope followed by the first non-Parkes FRB using the Arecibo telescope, and a few detections at ~ 0.8 MHz with the Green Bank Telescope (GBT) and the updated MOST (UTMOST) (**Table 2**). In the past year, the discovery rate has accelerated with the advent of widefield surveys using the Australian Square Kilometre Array Pathfinder (ASKAP) telescope in its “fly’s eye” mode at ~ 1.3 GHz (Shannon et al. 2018) and the Canadian Hydrogen Intensity Mapping Experiment (CHIME) cylinder array (CHIME/FRB Collab. et al. 2018) in the 0.4–0.8 GHz band. The CHIME detections (CHIME/FRB Collab. et al. 2019a,b) are the first to be found below 0.8 GHz and contrast with the nondetections of FRBs with the GBT at 0.35 GHz (Chawla et al. 2017) and the Low Frequency Array (LOFAR) at 0.15 GHz (Karastergiou et al. 2015). Burst detections are made on the basis of matched filtering (see the sidebar titled Matched Filtering).

When sky coverage and selection effects are accounted for, the small number of bursts detected from distinct sources translates into an astoundingly large all-sky rate Γ_{frb} (> 1 Jy ms) $\sim 10^3$ – 10^4 sky $^{-1}$ day $^{-1}$ above a 1 Jy ms fluence threshold³ (Thornton et al. 2013, Spitler et al. 2014, Champion et al. 2016, Keane & Petroff 2015, Oppermann et al. 2016, Scholz et al. 2016, Lawrence et al. 2017). Although different surveys yield rates that vary by about an order of

³1 Jy = 10^{-23} erg cm $^{-2}$ s $^{-1}$ Hz $^{-1}$ = 10^{-26} watts m $^{-2}$ Hz $^{-1}$.

Table 2 Low-frequency surveys

Telescope/Survey	\mathcal{F}_{\min} (Jy ms)	$\Omega_s T$ (deg 2 h)	N_{frb}	Γ_{frb} (sky $^{-1}$ day $^{-1}$)	References
LOFAR/ARTEMIS ^a 0.145 GHz	139	3.4×10^4	0	<29	Karastergiou et al. (2015)
GBT/GBNCC ^b 0.35 GHz	1.4	580	0	$<3.6 \times 10^3$	Chawla et al. (2017)
UTMOST 0.84 GHz	11	3.8×10^4	3	$78^{+12.4}_{-0.57}$	Caleb et al. (2016)
CHIME 0.4–0.8 GHz	TBD	TBD	13	NA	CHIME/FRB Collab. et al. (2019a)

^aReported $\mathcal{F}_{\min} = 62$ Jy \times 5 ms has been scaled to $W = 1$ ms using $\mathcal{F}_{\min} \propto \sqrt{W}$.

^bReported $\mathcal{F}_{\min} = 0.63$ Jy \times 5 ms has been scaled to $W = 1$ ms.

Abbreviations: ARTEMIS, Advanced Radio Transient Event Monitor and Identification System; CHIME, Canadian Hydrogen Intensity Mapping Experiment; GBT, Green Bank Telescope; GBNCC, Green Bank North Celestial Cap survey; LOFAR, Low Frequency Array; NA, not applicable; TBD, to be determined; UTMOST, the updated Molonglo Observatory Synthesis Telescope.

magnitude, allowance for survey thresholds, sky coverage, and small number statistics yields general consistency. The salient point is that the FRB rate is large, about 10^3 times greater than the GRB rate for FRB fluences larger than 1 Jy ms.

The Galactic latitude dependence of burst detection rates is of high interest because it would implicate propagation effects, especially interstellar scintillation (ISS), from the MW's ISM in the detectability of FRBs and estimated population sizes. However, the empirical evidence for latitude dependence is murky (Connor et al. 2016a). Early analyses suggested a deficit of mid-latitude FRBs that might be associated with the latitude dependence of ISS (Petroff et al. 2014, Macquart & Johnston 2015), which can more favorably enhance high-latitude detections. More recent analyses corroborate or assume a latitude dependence (Lawrence et al. 2017, Macquart & Ekers 2018b), whereas Bhandari et al. (2018) argue against it. This debate is based largely on studies of less than 20 objects from heterogeneous surveys. FRBs detected in directions through the Galactic plane do not seem to imply a low-latitude deficit. The repeating FRB 121102 (Spitler et al. 2014)

MATCHED FILTERING

Burst detection is based on the principle of matched filtering. A general model $I(\mathbf{X}, \boldsymbol{\theta}) = aA(\mathbf{X}, \boldsymbol{\theta}) + N(\mathbf{X})$ comprises a signal A , a design matrix of variables \mathbf{X} with dependence on a vector of parameters $\boldsymbol{\theta}$, a scale factor a , and noise N . If the noise is white, the matched filter is the signal shape, $A(\mathbf{X}, \boldsymbol{\theta})$. In practice, some aspects of the signal are known (e.g., dispersion delays), whereas burst shapes are not, requiring searches over a template bank of burst shapes. FRBs show stochastic structure that includes spectral confinement less than observing bandwidths and temporal substructure, knowledge of which can provide the basis for detection algorithms with better sensitivity.

The detection test statistic is the cross-correlation function (CCF) of the template, and events are found by requiring it to exceed a threshold. A Bayesian approach calculates the posterior probability distribution function (PDF) using priors and the likelihood function for the parameters $a, \boldsymbol{\theta}$.

Dispersed bursts have the form $I(t, v) = aA(v, t - t_{\text{DM}}(v) - t_0) + N(v, t)$, where t_{DM} is the dispersion delay and $A(v, t)$ is the shape in time and frequency. The parameters for this model are a, t_0, DM , and width W . The signal-to-noise ratio (S/N) of the CCF maximum is $A_{\max}\sqrt{W}/\sigma_N$ or, equivalently, $\mathcal{F}/\sqrt{W}\sigma_N$, where \mathcal{F} is the fluence (area of A), and σ_N is the root-mean-square (RMS) noise. In some cases, the true DM differs slightly from those found by maximizing the CCF.

and a new candidate FRB 141113 (Patel et al. 2018) were both found in the deep Arecibo pulsar survey, PALFA, covering a small field at low latitudes $|b| < 1^\circ$ in the Galactic anticenter direction. Detection of the latter FRB implies a large rate if it was found in the main lobe of the telescope beam, $\Gamma_{\text{frb}} (> 0.044 \text{ Jy}) = 7.8^{+27.2}_{-7.4} \times 10^4 \text{ sky}^{-1} \text{ day}^{-1}$, or a factor of ~ 5 smaller rate if instead the burst was found in a sidelobe. ISS and other selection effects are discussed in Section 3.

Recently, a shallow “fly’s eye” survey with very wide angular coverage using the ASKAP telescope (Shannon et al. 2018) yielded 20 large-amplitude bursts at 1.3 GHz, implying a rate $\Gamma_{\text{frb}} [> 26(W/1.26 \text{ Jy ms})^{-1/2}] = 37 \pm 8 \text{ sky}^{-1} \text{ day}^{-1}$ (Shannon et al. 2018). The survey’s narrow range of Galactic latitudes, $|b| = 50^\circ \pm 5^\circ$, minimized any latitude dependence as a factor in survey results. Comparison with deeper surveys and application of a V/V_m test both indicate a steep fluence dependence of the rate, $\Gamma_{\text{frb}} \propto F^{-2}$. This contrasts with other studies that indicate shallower dependences, $\Gamma_{\text{frb}} \propto F^{-0.6}$ (Vedantham et al. 2016a) based on a heterogeneous set of bursts, but is consistent with the analysis by Luo et al. (2018). As with the latitude dependence, knowledge of the rate’s dependence on fluence is currently limited by small samples of bursts whose positions within the telescope beam at the time of discovery are not known, leading to significant uncertainties on fluences. Surveys with interferometric arrays that also localize bursts (Law et al. 2015) will resolve this issue. We note that a previous fly’s eye survey with the Allen Telescope Array using smaller antennas (5-m versus 12-m diameter) and smaller aggregate on-sky time yielded no FRB detections (Siemion et al. 2012).

2.2. Follow-Up Observations: Trials and Tribulations

The directions of all FRBs have been searched for repeat bursts and several have been investigated in comprehensive multiwavelength observations. Follow-up observations from radio to γ -ray energies include those made as soon as possible after a radio burst detection using Astronomical Telegrams and an alert system based on VOEvents now under development (Petroff et al. 2017b). Panchromatic observations have yielded no burst detections and, apart from FRB 121102, no persistent counterparts (Palaniswamy et al. 2014, Petroff et al. 2015a, Scholz et al. 2016, Bhandari et al. 2018, Bower et al. 2018).

Several FRBs have shown repeat bursts at radio frequencies from ~ 0.4 to 8 GHz. FRB 121102, discussed in detail in Section 4, was found to repeat (Spitler et al. 2016) about 2.5 years after its initial detection (Spitler et al. 2014), but after only 10.3 h of total on-source time.

Some FRB lines of sight have been reobserved for more than 10^3 h without any redetections (e.g., Petroff et al. 2015b, Shannon et al. 2018), leading some authors to argue that most FRBs differ in physical nature from FRB 121102. If so, this would sustain the prospect that most FRBs are from one-off catastrophic events rather than from objects with persistent activity. However, if most or all FRBs ultimately repeat, the time to repeat may vary significantly between sources, particularly when amplitude distributions, scintillations and lensing, and detection thresholds are taken into account. To assess repeatability, the number of statistical trials in a large survey that yields multiple FRBs needs to be considered, and this depends on the (unknown) size of the source population in the sampled volume. The number of reobservations needed for repeat detections may be very large, especially in shallow surveys.

Consider a survey that yields N_d bursts from N_d distinct sources. Each of the M active sources in the surveyed volume repeats with an average rate η_1 . However, no repeats are detected even though each sky position is visited $N_v \gg 1$ times for a time T per visit. The total number of detected events is $N_d \sim \eta_1 T N_v M$. Because at most one event per source is seen in N_v visits, we have $\eta_1 T N_v \ll 1$. The number of reobservations N_{r_1} needed on average to redetect a single source is given by $\eta_1 T N_{r_1} = 1$. Using the survey yield, $N_{r_1} \sim N_v M / N_d$. But to have detected a single repeat

from any one of the N_d sources requires $\eta_1 TN_{r_1} N_d \sim 1$, which gives the number of repeats needed (per source) $N_{r_1} \sim N_v M/N_d^2$.

For the ASKAP survey (Shannon et al. 2018), $N_d = 20$, $T \sim 0.93$ h, and $N_v \sim 17$ to 1,308, corresponding to 16 to 1,200 h of reobservations. Using the median $N_v = 570$, the required number of reobservations to see a single repeat is $N_{r_1} \sim 1.4M$. A plausible fiducial population size sampled in the ASKAP survey is $M = 10^4 M_4$. Nicholl et al. (2017), for example, estimate a population number density $n_s \sim 10^4 n_{s4}$ Gpc⁻³, and the ASKAP survey may have sampled a volume of ~ 1 Gpc³. This implies that a much larger number of reobservations $\sim 10^4 M_4$ instead of the median 570 or the maximum $\sim 1,308$ reported by Shannon et al. (2018) is needed to expect any one of the ASKAP FRBs to have repeated in ASKAP observations.

Of course, higher sensitivity telescopes can significantly reduce the time-to-redetection ratio. From the survey, the implied burst rate per source is $\eta_1 \sim N_d/TN_v M \sim 3.8 \times 10^{-6} M_4$ h⁻¹, or about $0.033 M_4$ bursts per year, which is a very small rate. For a differential burst amplitude distribution $\propto S^{-\beta}$ for sources distributed uniformly in Euclidean space ($\beta = 5/2$), scaling from the ASKAP survey to the Parkes surveys, and assuming detection thresholds are bracketed by the distribution's cutoffs ($S_1 \ll S_{A,P} \ll S_2$), we obtain a predicted rate for Parkes observations $\eta_1(P) = \eta_1(A)(S_A/S_p)^{\beta-1} \sim 0.2\text{--}1.7 \times 10^{-3}$ h⁻¹ (for the nominal threshold or the fluence complete threshold, respectively), compared to a rate using the Arecibo telescope of $\eta_1(AO) \sim 0.065$ h⁻¹. These rates imply roughly 30 years, 600–4,800 h, and 15 h of reobservation between detections for the ASKAP, Parkes, and Arecibo surveys, respectively. Parkes (let alone ASKAP) reobservations have not reached the required time-to-redetection values, whereas the first repeat burst from FRB 121102 was found after 10.3 h of on-source time spread over ~ 2.5 years of elapsed time in Arecibo follow-up observations. The rates and repeat times estimated here are therefore consistent with sources distributed uniformly in Euclidean space that all produce multiple bursts. The possibility that all FRBs repeat removes a major argument for the conjecture that there are multiple populations of FRBs (Palaniswamy et al. 2018).

Some caveats on these estimates are needed. First, calculated yields assume all observations are statistically independent. This is not the case if burst rates or amplitudes are variable with correlation times longer than a typical observation time T . Episodic detections are expected if the correlation time is between T and the total span of observations on any FRB source. This is the case for FRB 121102, but it is not yet known if rate variations are intrinsic or due to propagation effects; this is discussed further in later sections. If $\eta_{1,i}$ is the intrinsic, Poisson burst rate per source and a large modulation lasting W_g occurring at intervals T_g is required to produce detectable bursts, the propensity for FRBs to occur singly (except for FRB 121102) implies $\eta_{1,i} W_g < 1$ and the apparent burst rate is $\eta_1 = \eta_{1,i} W_g / T_g$. For the repeater, η_1 during episodes lasting approximately days is much larger than the apparent rate, signifying that some kind of modulation is active that yields a variable mean burst rate (which may or may not correspond to Poisson statistics).

2.3. Dispersion and Scattering of FRBs

The arrival times of FRBs are inversely proportional to the line-of-sight integral of the group velocity. For a magnetized plasma the leading terms in the frequency-dependent part of the arrival time are (e.g., Tanenbaum et al. 1968, Tuntsov 2014, Suresh & Cordes 2019)

$$t(\nu) = 4.15 \text{ ms} \left(\frac{\text{DM}}{\nu^2} \right) \pm 28.6 \text{ ps} \left(\frac{\text{RM}}{\nu^3} \right) + 0.251 \text{ ps} \left(\frac{\text{EM}}{\nu^4} \right), \text{ (for } \nu \text{ in gigahertz)} \quad 1.$$

where terms are included up to second order in $(\omega_{p_e}/\omega)^2$ and linear in ω_{B_e}/ω (where ω_{p_e} and ω_{B_e} are the electron plasma and cyclotron frequencies, respectively). Each term has an associated

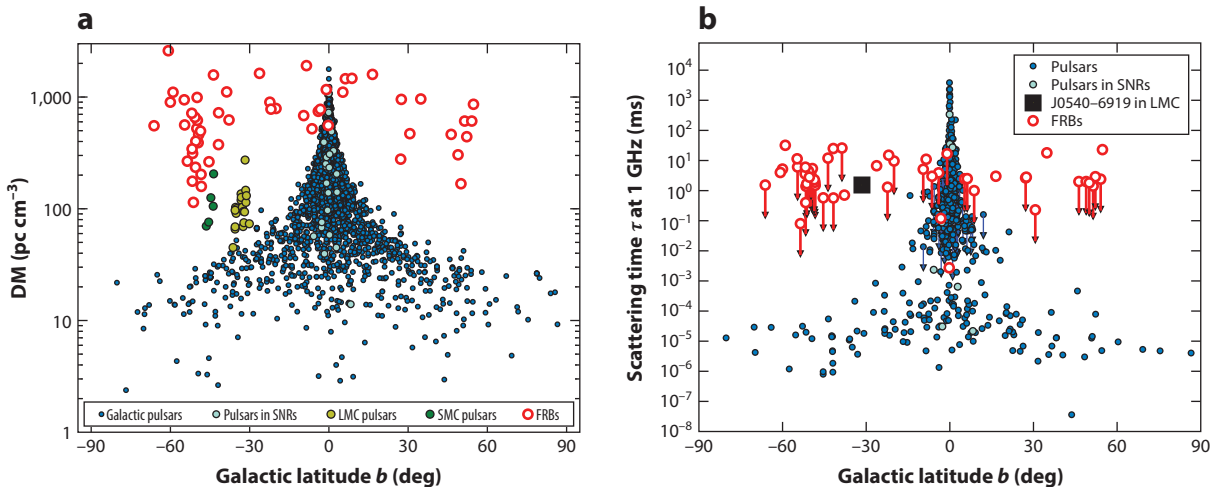


Figure 4

(a) Dispersion measures plotted against Galactic latitude for pulsars and FRBs. Different symbols are used for Galactic pulsars (2,422 objects), Galactic pulsars associated with SNRs (27), pulsars in the LMC (21) and SMC (5), and FRBs (55). (b) Scattering times for pulsars and FRBs at 1 GHz plotted against Galactic latitude. There are 421 pulsar measurements and 93 upper limits on τ compared with 18 FRB measurements and 37 upper limits. In panel a, DM measurements and pulsar associations were obtained from Manchester et al. (2005; <http://www.atnf.csiro.au/research/pulsar/psrcat>). Abbreviations: DM, dispersion measure; FRB, fast radio burst; LMC, Large Magellanic Cloud; SMC, Small Magellanic Cloud; SNR, supernova remnant.

line-of-sight integral measure. First is the dispersion measure DM (defined previously) with standard units of pc cm⁻³. The second term includes the Faraday rotation measure RM = 0.81 $\int ds n_e B_{\parallel}$ with standard units of rad m⁻² when the electron density n_e is in cm⁻³ and the parallel (to the line of sight) magnetic field is in microgauss units. The third involves the emission measure, EM = $\int ds n_e^2$, with standard units of pc cm⁻⁶. The two signs of the second term correspond to the two hands of circular polarization.

Early analyses of pulsars (Tanenbaum et al. 1968) and FRBs tested arrival times against the dispersion law $t(\nu) \propto \nu^{-\beta}$ and found $\beta = 2$ to within 1% or better (Thornton et al. 2013, Spitler et al. 2014, Champion et al. 2016, Keane & Petroff 2015, Scholz et al. 2016, Lawrence et al. 2017). The resulting upper limits on the ν^{-3} and ν^{-4} terms and the absence of free-free absorption (associated with EM) ruled out the association of FRBs with very dense plasmas (Dennison 2014, Katz 2014b, Luan & Goldreich 2014, Tuntsov 2014), such as stellar envelopes (Loeb et al. 2014). However, future observations of FRBs with large RMs may show distorted burst shapes at low frequencies $\nu \ll 1$ GHz due to the birefringent delays for the two hands of circular polarization.

Figure 4a shows DMs plotted against Galactic latitude b for FRBs and for pulsars in the MW and in the Large and Small Magellanic Clouds (LMC, SMC). Two conclusions can be made from the figure. First, the DMs of all FRBs with $|b| > 10^\circ$ are much larger than the outer envelope for Galactic pulsars that approximately follows a $\csc |b|$ dependence. An extragalactic population of FRBs would appear just this way if the total DM includes a large extragalactic contribution. Second, the DMs of FRBs cover a total range ~ 100 to 2,600 pc cm⁻³ that is comparable with the range for pulsars (3 to 1,700 pc cm⁻³), which is clearly due to the ISM of the Galaxy and in a few cases the ISM in the Magellanic clouds. The extragalactic contributions for the smallest DMs are equal to those expected from a dwarf galaxy, as indicated by the excesses seen in **Figure 4** for pulsars in the Magellanic clouds. The largest DMs are comparable with those expected either from a long path through the intergalactic medium (IGM) or a galaxy disk, from a galactic center

like that of the MW, or from a young supernova remnant (SNR; Piro 2016). Ionized gas in galaxies is therefore a plausible source for some or most of the extragalactic part of DM. We discuss the relative contributions to DM from host galaxies and the IGM in Section 7.

Figure 4b addresses FRB scattering. Temporal broadening of FRBs results from small-angle scattering by electron density variations on scales much larger than a wavelength. The scattered burst shape is the convolution of the emitted burst $\mathcal{F}(t)$ with an asymmetric pulse broadening function $p(t)$, such that $\mathcal{F}_s(t) = \mathcal{F}(t) * p(t)$. A one-sided exponential $p(t) = \tau^{-1} \exp(-t/\tau)\Theta(t)$ is often used for modeling of measured pulses but is a special case for thin scattering screens that only approximates realistic broadening functions. The scattering time is a strong function of frequency, $\tau \propto \nu^{-4}$.

The figure shows scattering times τ scaled to 1 GHz versus Galactic latitude for both pulsars and FRBs. Pulsar scattering times span more than ten orders of magnitude. The measured scattering times of FRBs, like their DMs, are also within the range spanned by pulsars, but they are much larger than those of pulsars at similar Galactic latitudes in most cases. This too is consistent with FRB scattering occurring primarily from extragalactic gas, at least for FRBs detected so far. However, only about 30% of the detected bursts show scattering. Section 7 discusses properties of the extragalactic plasma that underlie FRB scattering.

2.4. Time-Frequency Burst Structure

The earliest reported FRBs showed relatively simple temporal morphologies: Gaussian-like pulses modified in some cases by scattering broadening (Lorimer et al. 2007, Thornton et al. 2013, Spitler et al. 2014) with temporal substructure in one case (Champion et al. 2016). The present understanding is that featureless bursts are in part the outcome of the limited time resolution of post-detection dedispersion used in early surveys. Recent work enabled by coherent dedispersion of repeat pulses from FRB 121102 has revealed rich $t-\nu$ structure that differentiates some FRB bursts from their pulsar analogs. Examples are shown in **Figures 2** and **3**. The $t-\nu$ structure of FRBs is therefore substantially different from that of single pulses from pulsars, which tend to show only Galactic diffractive interstellar scintillation (DISS) but are otherwise continuous across a wide spectrum.

Frequency structure is best studied for the repeater FRB 121102 and is described in detail by Hessels et al. (2019). With adequate S/N, bursts from several FRBs show bandlimited structures of a few hundred megahertz sometimes combined with narrower frequency structure, which appears to be consistent with Galactic scintillation (DISS). The broader structure is not stable between bursts from the repeater, even changing over time separations of seconds and minutes. The broad structure appears anywhere in the 1.2- to 8-GHz frequency range used for studies of FRB 121102 though rarely in two broad receiver bands observed simultaneously (Law et al. 2017). Whether the broad structure is intrinsic to the radiation process or a post-emission propagation effect near the source (e.g., Cordes et al. 2017) is yet to be determined.

2.5. Polarization

Stokes parameters are available for a relatively small subset of FRBs (see **Table 3**). FRBCAT (currently) gives polarization information on five FRBs, with four showing significant linear polarization ranging from 8.5% to 80% and three showing circular polarization from 3% to 23%. The repeating FRB 121102 shows 100% polarization after removing Faraday rotation and FRB 180301 has $\sim 30\%$ linear polarization and $\sim 70\%$ circular polarization. These mixtures of linear and circular polarization are not dissimilar from those seen from pulsars. Polarization angles rotate across some FRBs by \sim tens of degrees (FRBs 110523 and 150418) while remaining constant in time

Table 3 Polarization of FRBs

FRB	% Linear	% Circular	RM (rad m ⁻²)	DM (pc cm ⁻³)	$\Delta\psi$ (deg)	References
110523	44 ± 3	23 ± 30	-186 ± 14	623	~ 40	Masui et al. (2015)
121102	100	0	1.03×10^5	560	<10	MJD 57747, Michilli et al. (2018)
			0.93×10^5		<10	MJD 57991
140514	0 ± 10	21 ± 7	ND	563	ND	Petroff et al. (2015a)
150215	43 ± 5	3 ± 1	1.5 ± 10.5	1,106	<20	Petroff et al. (2017a)
150418	8.5 ± 1.5	0 ± 4.5	36 ± 52	776	~ 70	Keane et al. (2016)
151230	35 ± 13	6 ± 11	0	960	ND	Caleb et al. (2018)
150807	80 ± 1	ND	12 ± 0.7	267	<20	Ravi et al. (2016)
160102	84 ± 15	30 ± 11	-221 ± 6	2,596	$\lesssim 10$	Caleb et al. (2018)
180301	~ 30	~ 70	$-3,100$	520	$\lesssim 20$	Price et al. (2018)

Abbreviations: DM, dispersion measure; ND, no data; RM, rotation measure.

for others to less than 20 degrees for FRBs 121102, 150215, and 150807. Pulsars generally show rotation across their pulses, often showing consistency with relativistically beamed emission from a spinning dipolar field (Backer et al. 1976). It is unclear if the position angles of FRBs indicate that the durations of FRBs are unrelated to a similar spinning radiation beam, that emission comes from nonspinning objects, or that polarization is induced as a propagation effect.

Four objects in the catalog have quoted RM values of which three are significant but only one, FRB 110523 (Masui et al. 2015), has an RM value that is consistent with arising from propagation through a host-galaxy disk. The total RM = -186 ± 14 rad m⁻²; only about 18 and 6 rad m⁻² are from the MW and IGM, respectively. The repeating FRB 121102 stands out by showing an extraordinarily large RM $\sim 10^5$ rad m⁻², which requires narrow frequency channels to resolve rotation of ψ with frequency. Initial studies at ~ 1.4 GHz showed no linear polarization because of Faraday depolarization across the coarse frequency channels. Only higher frequency observations allowed the Faraday rotation to be resolved. A final case is RM = $-3,100$ rad m⁻² for FRB 180301 (Price et al. 2018).

The wide range of RMs for FRBs is similar, perhaps coincidentally, to the range seen for Galactic pulsars, with the largest value (in magnitude) seen from the GC magnetar J1745–2900, RM $\approx -0.7 \times 10^5$ rad m⁻². And perhaps not so coincidentally, the RMs of both the GC magnetar and FRB 121102 have decreased in magnitude by significant amounts over periods of a few years: 5% for the magnetar (Desvignes et al. 2018) and 30% for the repeater (Michilli et al. 2018, and ongoing work). For both objects the accompanying change in DM is very small (<1%).

2.6. Localizations

As pointed out by various authors (e.g., Vedantham et al. 2016a, Eftekhari et al. 2018), subarcsecond localizations are required to identify host galaxies associated with FRBs at about gigaparsec distances. Rapid multiwavelength follow-up to detect the analog of GRB afterglows has not been fruitful (e.g., Petroff et al. 2017a), and the claimed rapidly fading radio transient associated with FRB 150418 (Keane et al. 2016) was shown instead to be common AGN variability (e.g., Williams & Berger 2016). In fact, multiwavelength observations that were simultaneous with burst detections from FRB 121102 have led to upper limits on high energy and optical emission associated with the bursts (Scholz et al. 2017, MAGIC Collab. et al. 2018).

The only reliable method so far is direct interferometric localization of the burst itself, as demonstrated for FRB 121102 (Chatterjee et al. 2017, Marcote et al. 2017). But for FRBs with small extragalactic contributions to their DMs, the number of candidate host galaxies in the error circles with large diameters (e.g., multiple arc minutes) may be small enough for identification of the FRB’s host (see, e.g., Mahony et al. 2018).

2.7. Energetics

With peak flux densities similar to those of pulsars, FRBs originating from gigaparsec distances compared with kiloparsec pulsar distances imply energy densities at the source and total burst energies that are larger by factors of $\sim 10^{10}$ to 10^{14} . For a flux density $S_v(t)$ in a bandwidth $\Delta\nu$, the energy density scaled to a distance $r = 10^{10} r_{10}$ cm from the source is

$$U_{\text{r,s}} \sim \frac{S_v \Delta\nu}{c} \left(\frac{d_{\text{so}}}{r} \right)^2 \approx 3.2 \times 10^{10} \text{ erg cm}^{-3} S_{v,\text{Jy}} \Delta\nu_{\text{GHz}} \left(\frac{d_{\text{so,Gpc}}}{r_{10}} \right)^2. \quad 2.$$

The equivalent magnetic energy $U_B = B^2/8\pi$ requires a field strength,

$$B \sim \left(\frac{8\pi S_v \Delta\nu}{c} \right)^{1/2} \frac{d_{\text{so}}}{r} \approx 9 \times 10^5 \text{ G} (S_{v,\text{Jy}} \Delta\nu_{\text{GHz}})^{1/2} d_{\text{so,Gpc}}, \quad 3.$$

that would be encountered, for example, at a distance r from a magnetar with a surface field $B = 10^{15} B_{15}$ G and radius $R = 10^6 R_6$ cm,

$$r \approx 3.3 \times 10^8 \text{ cm} R_6^{3/2} (B_{15}/d_{\text{so,Gpc}})^{1/2} (S_{v,\text{Jy}} \Delta\nu_{\text{GHz}})^{-1/4}. \quad 4.$$

Expressed in terms of the velocity of light cylinder radius $r_{\text{lc}} = cP/2\pi$ of a spinning object with period P ,

$$\frac{r}{r_{\text{lc}}} = 0.07 P^{-1/2} R_6^{3/2} (B_{15}/d_{\text{so,Gpc}})^{1/2} (S_{v,\text{Jy}} \Delta\nu_{\text{GHz}})^{-1/4}. \quad 5.$$

To match or exceed the radiation energy density with a particle energy density $U_p = \gamma m_e c^2$, electrons would have to be highly relativistic even with a large electron density. For example, a Lorentz factor $\gamma = (1 - \beta^2)^{-1/2} = 10^7$ (with $\beta = v/c$) requires an electron density $n_e \approx 4 \times 10^9 \text{ cm}^{-3}$ for the same parameters as in the above equations. The single-particle or particle-bunch radiation is therefore highly beamed into a solid angle $\Omega_b \sim \gamma^{-2}$. However, the total solid angle for an FRB is much larger than this because bursts are incoherent sums of many individual coherent units of radiation (Cordes & Wasserman 2016).

Isotropic emission implies a total emitted energy obtained by integrating over a spherical shell of thickness cW . Correcting for the beaming solid angle gives the burst energy $E_b \sim 4\pi S_v W \Delta\nu d_{\text{so}}^2 (\Omega_b/4\pi) \approx 1.2 \times 10^{39} \text{ erg} S_{v,\text{Jy}} W_{\text{ms}} \Delta\nu_{\text{GHz}} d_{\text{so,Gpc}}^2 (\Omega_b/4\pi)$. Small beam solid angles can therefore substantially alter burst energies.

2.8. Are Bursts From Rotation or Temporal Modulation?

If a rotating beam causes observed burst widths with duty cycle $W/P \leq 1$, the beam solid angle (in units of 4π) satisfies $\Omega_b/4\pi = \sin^2(\pi W/2P) \leq 1$. Small duty cycles imply $\Omega_b/4\pi \ll 1$, thus reducing energetic requirements for a burst. For this to be the case, pulse widths $W = 1 \text{ ms}$ require the spin period to exceed $P \gg 1.57 \text{ ms} W_{\text{ms}}$ to reduce the solid angle significantly. The total radiated energy also depends on the duration of radiation in the rotating beam. To avoid seeing multiple, periodic bursts, the duration must be less than a spin period, as for the repeating FRB, indicating

that there is substantial modulation of coherent radiation in the rotating frame. This also suggests that the observed burst durations themselves may be from temporal modulation rather than from a rotating beam. In this case, the beam solid angle cannot be constrained directly from observations.

2.9. Fast Transients, Brightness Temperatures, and Coherent Radiation

The radiation brightness temperature T_b is often used to characterize radio emission from astrophysical objects, and it is particularly useful for distinguishing incoherent and coherent emission. It is the effective blackbody temperature based on the Rayleigh–Jeans portion of the Planck spectrum $I_\nu = 2kT_b/\lambda^2$, where k is Boltzmann’s constant and $\lambda = c/v$ is the wavelength. For a transient burst of duration W and peak flux density S_{pk} , the specific intensity is $I_\nu \sim S_{\text{pk}}/\Omega_s$, where Ω_s is the observed solid angle of the source. A burst source of size $\sim cW$ at distance d subtends $\Omega_s \sim (cW/d)^2$, giving a brightness temperature $T_b \sim S_{\text{pk}}d^2/2k(vW)^2$. A 1-Jy FRB of millisecond duration yields $T_b = 3.4 \times 10^{35}$ K, compared to $T_b = 3.4 \times 10^{23}$ K for a Galactic pulsar at a kiloparsec distance.

Thermal sources (stars, HII regions) yield brightness temperatures equal to their physical temperatures. Nonthermal but incoherent emission such as synchrotron emission from AGNs yields T_b as large as $\sim 10^{12}$ K, indicating electron energies $kT_b = 86$ MeV. AGN radio emission is limited to about this brightness temperature by inverse Compton scattering.

Figure 5 shows the location of FRBs in the phase space for radio transients with a luminosity-like quantity⁴ $\mathcal{L} = S_{\text{pk}}d^2$ in Jy kpc² plotted against the dimensionless duration vW in gigahertz-seconds; these axes allow lines of constant brightness temperature to be drawn. The region of coherent sources is designated to the left of the $T_b = 10^{12}$ -K line that represents the approximate synchrotron-self-Compton limit for AGNs.

FRBs and pulses from pulsars necessarily involve coherent radiation and display propagation effects, including dispersive propagation, as described above, and DISS—the analog to optical scintillation of stars due to turbulence in Earth’s atmosphere—caused by turbulence in the interstellar electron density. Dispersion and scintillation are cofeatures because coherent sources are typically compact, allowing radiation to have short-enough durations to show dispersive propagation as well as scintillations.⁵ Coherent radiation mechanisms involve large numbers (N) of particles emitting with a distinct phase relationship, yielding collective power $\propto N^2$ rather than $\propto N$ for incoherent radiation. This can be through an antenna-type mechanism with charge bunching in coordinate space or through a plasma maser involving a nonmonotonic charge distribution in momentum space.

The signal processing of fast transients includes dedispersion that removes frequency-dependent delays to improve burst detection probabilities and to potentially restore bursts to their emitted shapes. Two dedispersion algorithms are used. The first, postdetection dedispersion, is approximate and shifts intensities by the dispersion delay for the center frequency of each channel of a digital filterbank. The best time resolution obtainable with this method at $\nu = 1.4$ GHz is Δt (μs) = $2\sqrt{8.3\text{DM}/v^3} \approx 110$ μs for $\text{DM} = 10^3$ pc cm⁻³ (Cordes & McLaughlin 2003), which is insufficient for probing burst time structure. The second method is coherent dedispersion (Hankins & Rickett 1975) that applies an exact matched filter to voltage data proportional to sampled electric fields. It corrects the $e^{ik(\nu)z}$ phase factor imposed by propagation and can provide submicrosecond resolution.

⁴ \mathcal{L} is usefully called the pseudo luminosity in pulsar contexts to emphasize that the measured flux density is influenced by both the angular width of the beam and its direction with respect to the line of sight.

⁵ ISS requires sources to be more compact than a critical (isoplanatic) angle in the same way that stars twinkle but planets do not, typically. Instead, pulsars and FRBs scintillate, but AGNs do not.

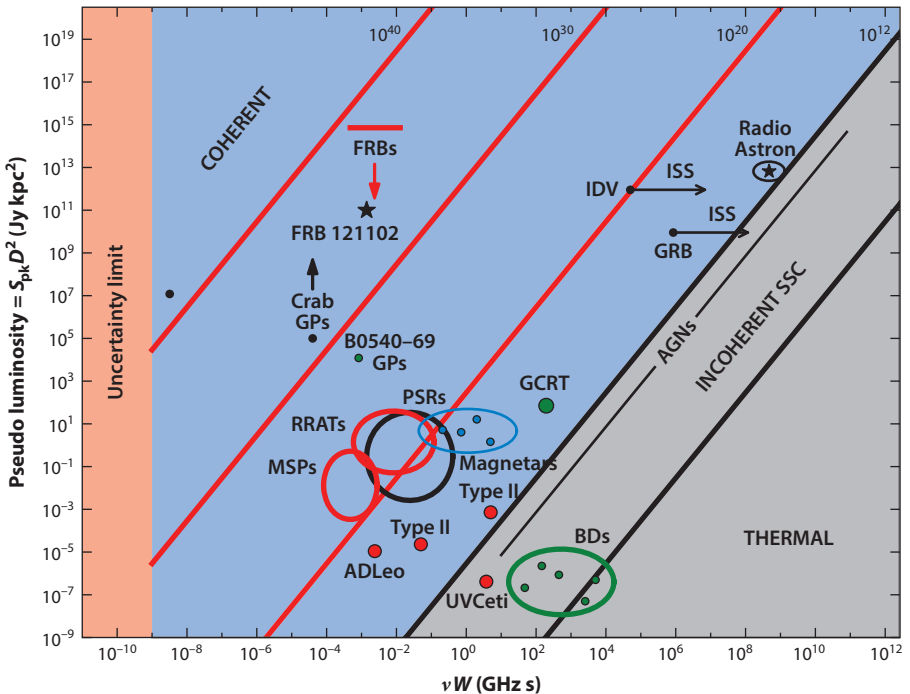


Figure 5

Time-luminosity phase space for radio transients showing the product of peak flux S_{pk} in Janskys and the square of the distance D in kiloparsecs versus the product of frequency ν in gigahertz and pulse width W in seconds. The “uncertainty” limit on the left indicates that $\nu W \gtrsim 1$, as follows from the uncertainty principle. Lines of constant brightness temperature $T_b = SD^2/2k(\nu W)^2$ are shown, where k is Boltzmann’s constant. Points are shown for the nanoshots (Hankins & Eilek 2007) and GPs detected from the Crab pulsar and a few millisecond pulsars, and single pulses from other pulsars. Points are shown for solar bursts, radio flares from stars, brown dwarfs, and AGNs. The regions labeled “coherent” and “incoherent” are separated by the canonical $\sim 10^{12}$ -K limit for the synchrotron self-Compton process occurring in AGNs. Arrows pointing to the right for the GRB and IDV points indicate that ISS implies smaller brightness temperatures than if characteristic variation times are used to estimate the brightness temperature. Fast radio transients include RRATs (McLaughlin et al. 2006), the GCRT source J1745-3009 (Hyman et al. 2005), and radio emission from Galactic magnetars (Olausen & Kaspi 2014). Abbreviations: AGN, active galactic nucleus; BD, brown dwarf; FRB, fast radio burst; GCRT, Galactic center radio transient; GP, giant pulse; GRB, gamma-ray burst; IDV, intraday variable; ISS, interstellar scintillation; MSP, millisecond pulsar; PSR, pulsar radio source; RRAT, rotating radio transient; SSC, synchrotron self-Compton.

3. THE ASTRO-OPTICS OF FRBs

The detectability of FRBs and their observed properties are strongly affected by propagation through intervening plasmas and mass assemblies. We summarize propagation phenomena that affect FRB surveys and also how they can be used to probe FRB sources, their environments, and the IGM, including dark matter.

3.1. Galactic Propagation

Electron density variations δn_e in the ionized ISM cause three important effects: angular broadening (seeing), pulse broadening due to angular broadening, and intensity scintillations from both refraction and diffraction. Length-scales smaller than the Fresnel scale $\sim \sqrt{\lambda d/2\pi} \sim 10^6$ km diffract

radiation, whereas refraction, caustics, and multiple images from larger scales can strengthen and dim bursts and affect arrival times. For reviews, see Rickett (1990) and Narayan (1992).

An extragalactic burst viewed through the Galaxy's ISM is broadened into an angular diameter θ_G and temporally smeared by $\tau_G \sim d_{lo}\theta_G^2/8\ln 2c$, where $d_{lo} \sim L_g$ is the distance of the scattering layer from the observer, approximately the Galactic scale height ~ 1 kpc of free electrons. The upper envelope of values and the latitude dependence of τ_g in **Figure 4** correspond to a Galactic seeing diameter, $\theta_G \sim 0.3$ mas $\times \sin |b|^{-3/5} v^{-2.2}$, where the exponents are for a medium with a Kolmogorov wavenumber spectrum for δn_e . Galactic seeing is important for any gravitational nanolensing of FRBs (e.g., Eichler 2017) because it may exceed the Einstein radius for dark matter objects and contaminate gravitational time delays.

Intensity scintillations (DISS) are correlated over a bandwidth $\Delta\nu_d$ related to τ by an uncertainty relation $2\pi\Delta\nu_d\tau \approx 1$ (Cordes & Rickett 1998, Lambert & Rickett 1999). These scintillations are accompanied by refractive interstellar scintillation (RISS), though typically DISS is more important. In the strong scintillation regime where $\Delta\nu_d \ll \nu$, DISS is 100% modulated with an exponential gain PDF, $f_g(g) = \exp(-g)\Theta(g)$, where $\Theta(g)$ is the Heaviside function (0 for $g < 0$, 1 otherwise).

3.2. Propagation Model for Bursts

The simplest model for an individual burst relates the emitted (pseudo) luminosity $\mathcal{L}(\nu, t)$ to the measured flux density $S(\nu, t)$ using the distance d , a propagation modulation $g(\nu, t)$, and a composite delay $t_d(\nu, t)$ primarily from dispersion, scattering, and refraction,

$$S(\nu, t) = d^{-2} g(\nu, t) \mathcal{L}[\nu, t - t_d(\nu, t)]. \quad 6.$$

Many of the observed properties of FRBs are likely a combination of the intrinsic (to the source) $\mathcal{L}(\nu, t)$ and the extrinsic $g(\nu, t)$, but their relative contributions have not yet been disentangled satisfactorily. The modulation g has both short-term and long-term contributions from Galactic DISS (minutes to hours) and Galactic RISS (hours to months), respectively. Plasma lensing in host galaxies and gravitational microlensing will have similarly long timescales. The episodic bursting of FRB 121102 is naturally explained if bursts are heavily modulated by g even if \mathcal{L} is a process with fixed mean rate (Poissonian or otherwise). Variability of the total delay t_d could potentially account for the observed aperiodicity for a source that is intrinsically periodic. Of course, these features might also be intrinsic.

3.3. Scattering in Host Galaxies, Intervening Galaxies, and the Intergalactic Medium

The broadening times measured for FRBs (**Figure 4**) are extragalactic and highly likely to be from scattering in host galaxies. However, there is debate about the relative roles of host-galaxy scattering and contributions from the IGM (e.g., Macquart & Koay 2013, Luan & Goldreich 2014, Cordes et al. 2016, Xu & Zhang 2016). Scattering near FRB sources yields a broadening time $\tau_h \sim d_{sl}\theta_h^2/8\ln 2c$, where $d_{sl} = L_h$ is the scale height or source-scattering layer distance and θ_h is the range of angles over which radiation is scattered. However, the scattering diameter seen by an observer is much smaller (and typically unmeasurable), $\theta_o = (d_{sl}/d_{so})\theta_h \ll \theta_h$, where d_{so} is the source–observer distance.

Intervening galaxies are likely only for $z \gtrsim 1$. They will contribute to the total DM (perhaps modestly) but may broaden bursts by scattering by large amounts because of the long path lengths. The Euclidean expression $\tau_g \sim (d_{sl}d_{lo}/d_{so})\theta_g^2/8\ln 2c$ holds in flat Λ CDM space, where d_{sl} , d_{lo} , and d_{so} are angular diameter distances; τ_g increases by a factor of $(1 + z_g)$ while θ_g

decreases by $(1 + z_g)^{-2}$ (for a plasma). The seeing disk diameter for a face-on MW galaxy will be $\theta_g \sim 0.8(1 + z_g)^{-2}$ mas, giving a very large scattering time $\tau_g \sim 560\text{ ms} (1 + z_g)^{-3} (d_{\text{sl}} d_{\text{lo}} / d_{\text{so}})$ for distances in gigaparsecs that will render undetectable all but the strongest bursts.

In principle, the IGM can contribute to the scattering of FRBs if long path lengths compensate for the tenuous electron density. The scattering time per unit length depends on the square of the electron density, and thus $\tau \propto \text{DM}^2$ with a proportionality constant dependent on the length scales of density fluctuations and on the filling factor of larger-scale density concentrations. Luan & Goldreich (2014) and Macquart & Koay (2013) argue that the diffuse IGM has properties that yield negligible scattering. This conclusion is consistent with the lack of any obvious correlation of the scattering time with the extragalactic DM (Cordes et al. 2016; see also Section 7.3).

IGM structures including Lyman- α clouds, damped Ly- α systems, and intracluster media will have larger electron densities, different filling factors, and smaller length scales than the diffuse IGM, so scattering in those regions may be significant (Macquart & Koay 2013; but see Prochaska & Neeleman 2018). At present, there is no evidence for scattering from such regions. In fact, for a few FRBs, fine-scale spectral structure is consistent with Galactic DISS and requires that the extragalactic scattering originate from near the FRB source (within a galaxy radius) (e.g., Masui et al. 2015).

3.4. Propagation Factors that Affect FRB Detections

The amplitudes of bursts may be influenced strongly by lensing, scintillation, and absorption. Such effects need to be considered in analyses of both surveys and follow-up observations.

3.4.1. Scintillation modulations and quenching. DISS typically reduces the burst amplitude but occasionally can boost it by a large amount for large, less probable gains on the tail of the exponential distribution, $f_g(g) = e^{-g}$. The role of such modulations in burst detections (or missed detections) depends on the number of statistical trials in an FRB survey. This in turn depends on the size of the burst source population and the number of bursts emitted per source. If many trials are done, detected bursts may have been boosted significantly by DISS (or lensing, as discussed below), with the corollary that repeat bursts will also have low probability.

However, DISS modulations are reduced if observations are made with bandwidths much larger than their correlation bandwidth or if the effective source size is larger than a critical amount. A finite bandwidth ($\Delta\nu$) reduces the RMS modulation of g from unity to $m_B \approx 2\sqrt{\Delta\nu_d/\Delta\nu}$ for a correlation bandwidth $\Delta\nu_d \ll \Delta\nu$. **Figure 6a** shows the correlation bandwidth for a few frequencies versus Galactic latitude, demonstrating that $\Delta\nu_d$ plummets to very small values at low latitudes and that DISS is largely quenched (for large observing bandwidths), disallowing large scintillation boosts.

Similarly, a finite source size θ_x reduces the modulation to $m_\theta \approx \theta_{\text{iso}}/\theta_x$, where θ_{iso} is a critical (isoplanatic) angular scale (see the sidebar titled Scintillation Source Size Requirements). Sources of millisecond bursts are necessarily small enough to show fully modulated Galactic DISS. However, any extragalactic scattering can make the apparent size larger than θ_{iso} and, thus, quench DISS. In a few cases, Galactic DISS has been identified in FRB spectra, indicating that the extragalactic scattering also seen must occur in or near their host galaxies (Masui et al. 2015, Ravi et al. 2016, Gajjar et al. 2018, Spitler et al. 2018). **Figure 6b** shows the distance constraints on a scattering screen in order for DISS to be manifest. The occurrence of Galactic DISS is therefore a useful probe of the host galaxies and environments of FRB sources.

3.4.2. Reduction in survey sensitivity from free-free absorption and pulse broadening. Dispersing and scattering electrons also absorb FRBs. Apart from directions through the inner

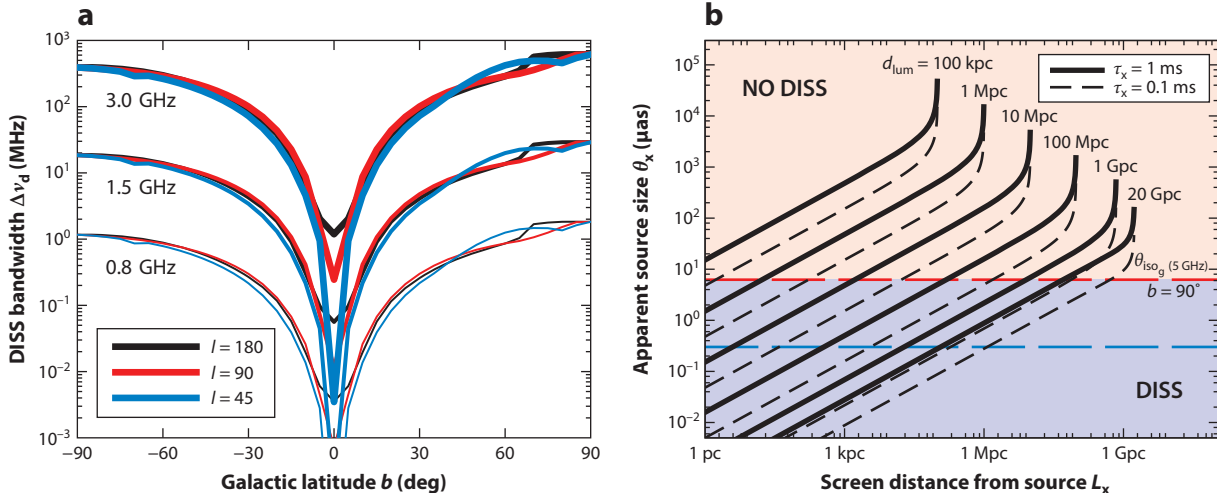


Figure 6

(a) DISS bandwidth versus Galactic latitude for several combinations of Galactic longitude and radio frequency, as labeled. The curves are calculated using the NE2001 electron density model. (b) Apparent size of FRB source from extragalactic scattering versus distance of an extragalactic scattering screen from the source. The intrinsic source size is assumed negligible. Solid lines are for an FRB scattering time of 1 ms, and dashed lines are for 0.1 ms. Pairs of curves are shown for source luminosity distances of 100 kpc to 20 Gpc. The dashed horizontal lines indicate the critical angular size (isoplanatic angle $\theta_{\text{iso}}(5 \text{ GHz})$) at the labeled frequencies for the North Galactic pole ($b = 90^\circ$). Apparent source sizes above this line will have strongly attenuated DISS from scattering in the Milky Way, as indicated by the shading and the label “NO DISS.” Cosmological effects are relevant only for source distances greater than a few gigaparsecs. Abbreviations: DISS, diffractive interstellar scintillation; FRB, fast radio burst.

Galaxy at low frequencies, free-free absorption will only be important for any dense gas in host galaxies and for low-frequency observations ($\lesssim 300$ MHz). The EM is related to the DM and path length L_h of the host along with parameters ζ and ϵ that quantify electron density fluctuations (Cordes et al. 2016),

$$\text{EM}_h = \frac{\zeta(1 + \epsilon^2)\text{DM}_h^2}{fL_h} \sim 10^4 \text{ pc cm}^{-6} \times \frac{\zeta(1 + \epsilon^2)}{fL_{h,\text{pc}}} \left(\frac{\text{DM}_h}{100 \text{ pc cm}^{-3}} \right)^2, \quad 7.$$

corresponding to an optical depth (Draine 2011)

$$\tau_{\text{ff}} = \frac{3.37 \times 10^{-3}}{T_4^{1.3} \nu^{2.1}} \frac{\zeta(1 + \epsilon^2)}{fL_{h,\text{pc}}} \left(\frac{\text{DM}_h}{100 \text{ pc cm}^{-3}} \right)^2. \quad 8.$$

Although negligible at 1 GHz for the nominal DM_h , the optical depth can exceed unity for larger host-galaxy DMs and lower frequencies. Free-free absorption may therefore affect detection rates of low-frequency surveys and may provide an additional probe of source environments.

Pulse broadening, when either τ_G or τ_x is comparable with or larger than the intrinsic burst width W , reduces detection numbers in surveys. It conserves fluence, so the matched-filter output amplitude is reduced by a factor,

$$f_\tau(\nu, l, b) = (1 + 2\tau^2/W^2)^{-1/4} \approx \left(W/\sqrt{2}\tau \right)^{1/2} \quad \text{for } W \ll \tau. \quad 9.$$

The scattering time and intrinsic width W are implicitly frequency dependent and τ is strongly direction dependent, as implied in **Figure 6a** and using $\tau \propto \Delta\nu_d^{-1}$. The scattering factor

SCINTILLATION SOURCE SIZE REQUIREMENTS

DISS has extraordinary resolving power because it is quenched for sources larger than about a microarcsecond. Waves from a source of angular size θ_x have a coherence length $l_c \sim \lambda/\theta_x$ on a Galactic scattering screen. The coherence length must exceed the patch size on the screen that contributes to measured flux densities, or $\theta_s < \theta_{\text{iso}} = \lambda/\theta_G d_{\text{lo}}$. For Galactic scattering with $d_{\text{lo}} = 1$ kpc and $\theta_G = 1$ mas, the isoplanatic angle is $\theta_{\text{iso}} = 0.4$ μas. Pulsars easily satisfy this constraint as do FRBs, which are intrinsically smaller in angular size by a factor $\sim 10^{-6}$ given their millisecond durations and gigaparsec distances. However, scattering in host or intervening galaxies reduces the coherence length and can quench scintillations. Let θ_x and θ_G be the scattering diameters produced by extragalactic and Galactic screens at distances L_x and L_G from the source and observer, respectively, and τ_x and τ_G the corresponding broadening times; then the requirement becomes (for ν in gigahertz; L_x and L_G in kiloparsecs; and d_{so} in gigaparsecs),

$$\theta_x \theta_G \lesssim \frac{4 \ln 2}{\pi} \frac{\lambda}{L_G} \sim \frac{(19.1 \text{ μas})^2}{(\nu L_G)} \quad \text{or} \quad \tau_x \tau_G < \frac{1}{(2\pi\nu)^2} \frac{d_{\text{so}}^2}{L_x L_G} \approx (0.16 \text{ ms})^2 \left(\frac{d_{\text{so}}^2}{\nu^2 L_x L_G} \right).$$

Host-galaxy scattering can also quench gravitational microlensing, as discussed in Section 3.4.4.

undoubtedly plays a prominent role in low-frequency (<0.8 GHz) surveys and surveys of the inner Galaxy at low latitudes.

3.4.3. Aggregate frequency-dependent factors relevant to FRB detection. Figure 7 presents the aggregate effects from propagation of FRBs through ionized gas as a function of frequency. Figure 7a shows bandwidth and source-size quenching. The bandwidth reduction

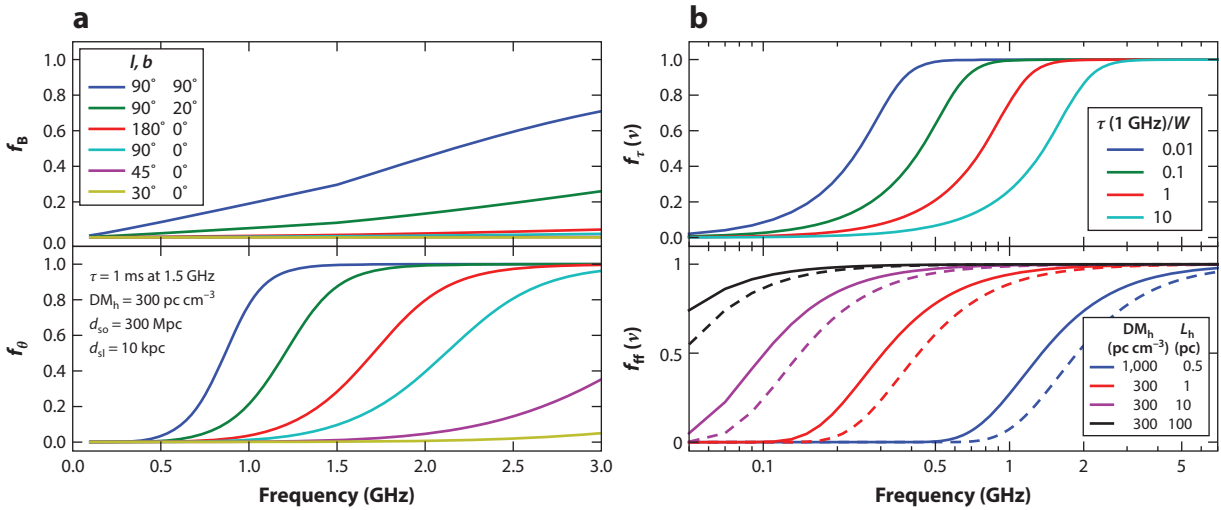


Figure 7

(a) DISS reduction factors due to bandwidth averaging for different directions specified in Galactic coordinates (*upper panel*) and due to quenching of Galactic DISS from source-size quenching by scattering at 10 kpc from the FRB source (*lower panel*). (b) (*Upper panel*) S/N reduction factors from pulse broadening. Curves are shown for different ratios of pulse broadening time τ to intrinsic burst width W at 1 GHz. (*Lower panel*) Solid curves give the factor f_{ff} from free-free absorption in a host galaxy for different values of DM_h and clump thickness L_h and with no internal density fluctuations in the clump ($\epsilon = 0$), as labeled. Dashed lines are for full density modulations ($\epsilon = 1$). Abbreviations: DISS, diffractive interstellar scintillation; DM, dispersion measure; FRB, fast radio burst; S/N, signal-to-noise ratio.

factor in the upper frame is evaluated for six different directions and for 10% receiver bandwidths. The bottom frame shows the source-size reduction factor caused by extragalactic scattering. The pulse-broadening time due to scattering is held fixed to $\tau = 1$ ms at 1.5 GHz and scales as $v^{-4.4}$, and the apparent angular size of the source is calculated assuming a 10-kpc separation of the scattering region and source. The conclusion is that if Galactic DISS is important in survey detections of FRBs, by either boosting or suppressing burst amplitudes, it will be much less important (if not negligible) at low frequencies. Suppression of FRB amplitudes is shown in **Figure 7b**. The upper frame shows the suppression factor due to pulse broadening $f_\tau(v)$ for four values of the ratio τ/W referenced to 1 GHz. Suppression of S/N occurs at low frequencies even if scattering is not evident at 1 GHz. The bottom frame shows the attenuation from free-free absorption, $\exp(-\tau_{\text{ff}})$, that can, but need not, be important at low frequencies.

3.4.4. Plasma and gravitational lensing. Refraction and especially lensing from discrete structures cause multiple imaging from the Crab pulsar (Graham Smith et al. 2011), strong enhancements of pulse amplitudes from the bow shock produced by a millisecond pulsar (Main et al. 2018), fringes in the dynamic spectra of pulsars (Wolszczan & Cordes 1987), and events in the radio light curves of AGNs (Fiedler et al. 1987, Bannister et al. 2016). The strongly episodic burst detections from the repeating FRB 121102 may be explained most easily from plasma lensing, and the overall detection rate could also be affected. Plasma lensing involves diverging or converging rays from refraction by electron density enhancements or deficits, respectively. These can produce strong dimming or large amplifications from caustics along with arrival time and DM variations (Cordes et al. 2017; see also Katz 2014b).

A Gaussian lens with a dispersion measure profile $\text{DM}(x) = \text{DM}_\ell e^{-x^2/\alpha^2}$ produces multiple images and caustics for lens–observer distances larger than a frequency-dependent focal distance $d_f(v)$. The focal distance is ~ 1 Gpc for a modest lens with $\text{DM}_\ell = 1 \text{ pc cm}^{-3}$ and $\alpha = 1 \text{ AU}$ at, say, a 1-pc distance from an FRB source at 1 Gpc from the Earth. Amplifications as large as ~ 100 are plausible. Equivalently, caustics will be seen for frequencies less than a focal frequency $v_f \sim 1.2 \text{ GHz}$ for the same nominal parameters.

The lens gain and the number of images are strong functions of frequency as well as observer location. The dependence of the lens gain on the observer’s location and frequency is shown in **Figure 8** for a one-dimensional Gaussian lens perturbed with 10% oscillations. Numerous caustics occur in this case, and the gain is strongly peaked in frequency for some observer locations, whereas at others the gain is $\ll 1$. The observer’s effective location can change owing to motion of the source or lens (as well as the observer), serving as a possible explanation for the absence of bursts from the repeating FRB at some epochs.

Gravitational lensing can also amplify FRBs and impose delays between multiply imaged bursts, which may also produce interference effects in dynamic spectra. Sources with projected sizes $d_{\text{lo}}\theta_s$ and impact parameters b much smaller than the Einstein radius, $R_E = (4GM/c^2)^{1/2}(d_{\text{sl}}d_{\text{lo}}/d_{\text{so}})^{1/2}$, can show double images with large amplifications $A \sim R_E/b \gg 1$ for durations $\Delta t \sim 2R_E/v_{\perp}A$ for an effective transverse speed v_{\perp} . The probability of amplifications greater than A is $P(>A) \sim \pi R_E^2 L n_*/A^2$ for a population of lensing masses M with a number density n_* in a region of depth L .

Lensing from a stellar population in a host galaxy with $d_{\text{sl}} \ll d_{\text{so}}$ has Einstein radius $R_E \sim 4 \text{ AU} (M/M_\odot)^{1/2} d_{\text{sl}} (\text{kpc})^{1/2}$, duration $\Delta t \sim 0.1 \text{ year} (M/M_\odot)^{1/2} d_{\text{sl}} (\text{kpc})^{1/2} (Av_{100})^{-1}$ for $v_{\perp} = 100v_{100} \text{ km s}^{-1}$, and $P(>A) \sim 10^{-6} A^{-2} (M/M_\odot) L_{\text{kpc}} n_*(\text{pc}^3)$. Microlensing might enhance a few bursts out of a much larger number of unlensed events from many host galaxies. However, given the small $P(>A)$, microlensing is inconsistent with the episodic detections of FRB 121102 unless a particular geometry allows repeated lensing.

If it occurs for any FRBs, gravitational lensing is a unique diagnostic for dark matter comprising primordial black holes (PBHs) or other discrete objects, including those in binaries

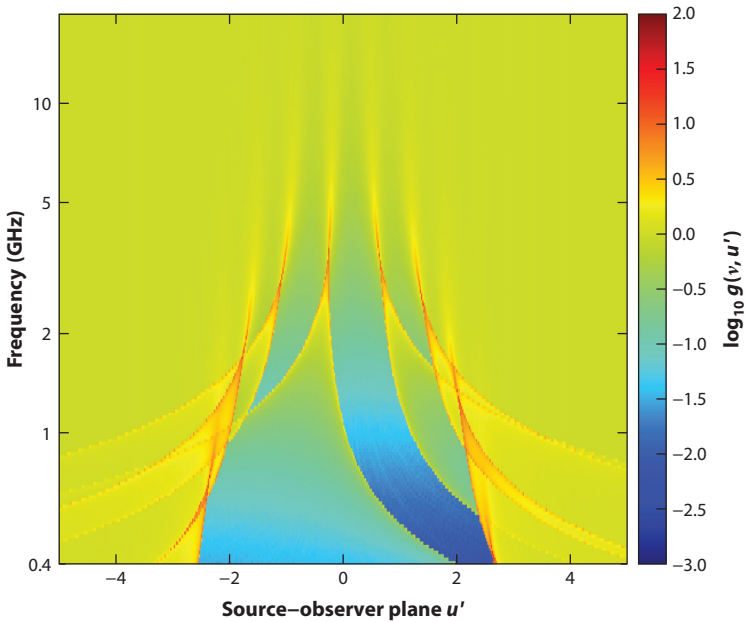


Figure 8

Lens gain versus dimensionless observer position u' and radio frequency for a lens with sinusoidal perturbations of a Gaussian DM profile, $\text{DM}_\ell(x) = [1 + 0.1 \sin(5x + \phi)]$. The color bar represents $\log_{10} g(v, u')$ and indicates that gain excursions range from 10^{-3} to 10^2 . Abbreviation: DM, dispersion measure.

(Wang & Wang 2018). Point-mass lensing yields a differential delay between a dual-imaged burst, $\Delta t_\ell \sim (8GM/c^3)(1+z_\ell)/A = 39\ \mu\text{s} (1+z_\ell)(M/M_\odot)/A$ for $A \ll 1$ (Zheng et al. 2014, Muñoz et al. 2016). This may be detectable as an oscillation in dynamic spectra for bursts that are coherently dedispersed, providing a fringe pattern of the form $\cos 2\pi v \Delta t_\ell$ with an amplitude related to the image amplification ratio (Zheng et al. 2014, Eichler 2017). Objects with masses $\gtrsim 0.1 M_\odot$ are within reach. At present, none of the spectral features seen in FRBs is clearly associated with a fringe pattern but more detailed analyses, particularly with wideband spectrometers, are needed. PBHs with masses $\sim 30 M_\odot$ may be strongly constrained with large FRB samples if they extend to $z \gtrsim 0.5$ because the event probability can be large enough (~ 0.02) if PBHs comprise a significant fraction of dark matter (Muñoz et al. 2016). Lensing from intervening galaxies (Li et al. 2018b) has been discussed as a means for determining cosmological parameters, including H_0 and the spatial curvature Ω_k . Such lensing will be sustained for long times and cannot account for the episodicity of the repeater FRB 121102.

4. THE REPEATING FRB 121102

The detection of FRB 121102 (Spitler et al. 2014) in observations acquired at the Arecibo observatory on November 2, 2012 (Figure 1), laid to rest any residual concerns about site-specific interference at the Parkes observatory (Petroff et al. 2015c) and confirmed the astrophysical nature of the FRB phenomenon. As with other FRBs, the measured DM of $557.4 \pm 2.0 \text{ pc cm}^{-3}$ significantly exceeded the predicted line-of-sight maximum electron density contribution from the MW (188 pc cm^{-3}), although the location of the source at a low Galactic latitude in the Galactic anticenter ($\ell, b = 174.95^\circ, -0.22^\circ$) added significant uncertainty, requiring extensive

multiwavelength investigation to place deep limits on Galactic HII regions along the line of sight (Scholz et al. 2016).

The detection of additional bursts from FRB 121102 (Spitler et al. 2016) was an unexpected payoff to routine follow-up observations (**Figure 3**). The overlapping sky position uncertainty regions and the consistent value of DM unambiguously identified FRB 121102 as a repeating source and ruled out cataclysmic and explosive models as the source of (at least) that particular set of FRB events.⁶

The repetition of the bursts, though sporadic (see Section 4.2), enabled a targeted observation campaign with the Karl G. Jansky Very Large Array (VLA), where interferometric visibilities were acquired at high resolution in both time and frequency ($\Delta t = 5$ ms, $\Delta\nu = 4$ MHz over a bandwidth of 1 GHz, limited by the maximum data rate of ~ 300 MB s $^{-1}$). In 83 h of observations over 6 months, nine bursts were detected, leading to a precise source localization on the sky ($\alpha, \delta = 05^{\text{h}}31^{\text{m}}58.70^{\text{s}}, +33^{\circ}08$ arcmin 52.5 arcsec with an uncertainty of ~ 0.1 arcsec; Chatterjee et al. 2017). The detections used complementary approaches, dedispersing the visibilities at the known DM of the FRB and then searching for a transient source in a sequence of 5-ms images (e.g., Law et al. 2015), as well as phasing and summing visibilities to create time–frequency dynamic spectra over a grid of sky positions and searching those for single dispersed pulses.

Chatterjee et al. (2017) identified a variable radio source coincident with the sky position of the bursts (**Figure 9**), with a mean flux density of ~ 190 μJy ; the nature of this persistent radio source (hereafter PRS) remains enigmatic and is discussed below (Section 4.1). Building on the initial localization, Marcote et al. (2017) used very long baseline interferometry with Arecibo and the European VLBI (Very Long Baseline Interferometry) Network to detect bursts, localize them with ~ 12 -mas precision, and confirm their spatial coincidence with the PRS. Chatterjee et al. (2017) also identified a faint optical counterpart to the bursts, with Sloan Digital Sky Survey (SDSS) r' -band magnitude $m_{r'} = 25.1$ AB mag. With optical imaging and spectroscopy at the 8-m Gemini North telescope, Tendulkar et al. (2017) classified the counterpart as a low-metallicity star-forming dwarf galaxy and measured a redshift $z = 0.19273(8)$, corresponding to a luminosity distance of 972 Mpc (**Figure 10**). With high-resolution optical and IR imaging using the *Hubble Space Telescope* and the *Spitzer Space Telescope*, Bassa et al. (2017) further showed that the emission is dominated by a bright knot of star formation in the irregular dwarf galaxy with a half-light diameter of 1.4 kpc, compared to 5–7 kpc for the galaxy itself, and this knot coincided (within the astrometric frame-matching uncertainties) with the PRS. With its high specific star-formation rate, low metallicity, and prominent emission lines, the host galaxy resembles the preferred hosts of long-duration GRBs and superluminous supernovae (SLSNe; e.g., Fruchter et al. 2006, Perley et al. 2013, Vergani et al. 2015, and others), as discussed further below (Section 5).

Unlike GRBs and SNe, though, the bursts from FRB 121102 show no afterglows and have been observed to repeat at short enough intervals that no plausible explosive mechanism (i.e., one that destroys the central engine) could power them. For example, Gajjar et al. (2018) report 18 bright bursts detected by the GBT at 4–8 GHz within just a 30-minute span [and many more faint ones were identified by Zhang et al. (2018) in the same span of data]. Additionally, simultaneous coverage in X-rays (Scholz et al. 2017) and high-energy gamma rays (MAGIC Collab. et al. 2018) as well as optical wavelengths reveals no other coincident electromagnetic emission with bursts from FRB 121102.

However, the well-localized sky position and DM allow coherently dedispersed observations of FRB 121102 over a broad range of radio frequencies and a long period of time. Such broadband,

⁶It also introduced a point of confusion in the nomenclature, because prior usage had made no distinction between the burst event and its source. At present, there are a handful of examples of repeating sources, and the confusion remains unresolved except by context.

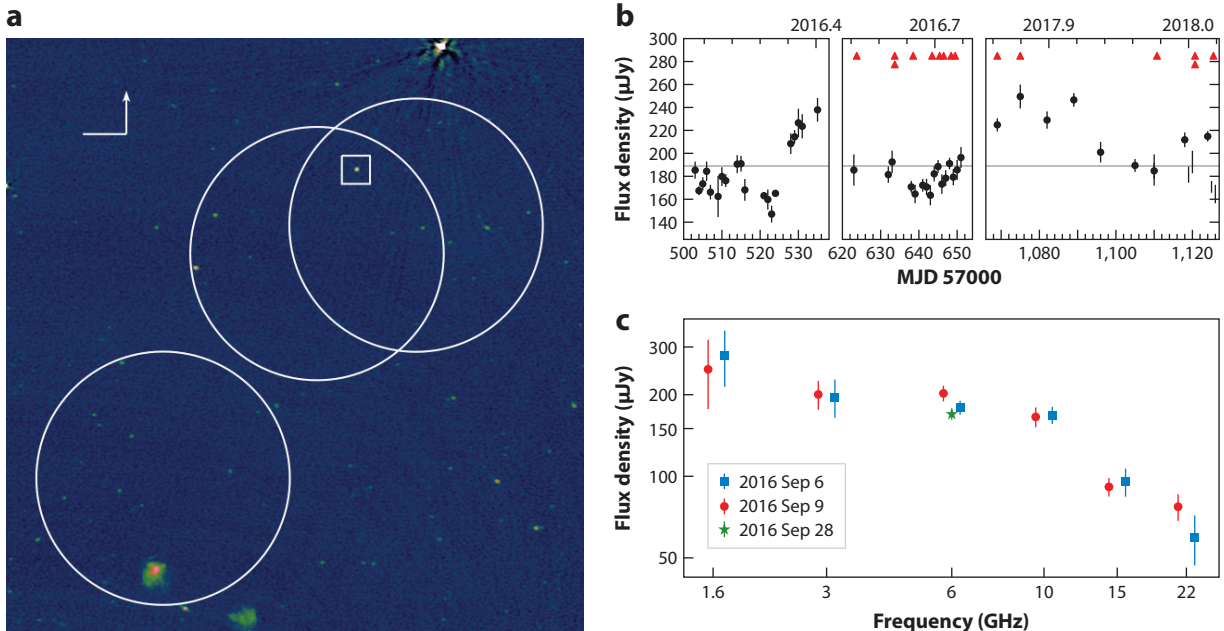


Figure 9

VLA observations of the field of FRB 121102. (a) VLA image at 2–4 GHz with 2 arcsec resolution and an image RMS of 2 μ Jy (Chatterjee et al. 2017). Arecibo detection beam positions and sizes are indicated with white circles, illustrating the positional uncertainties. The radio counterpart (PRS) is enclosed by a 20-arcsec square within the beam overlap area. (b) The light curve of the PRS, from observations reported by Chatterjee et al. (2017) and new observations, indicating the source variability. The average source flux density of $\sim 190 \mu$ Jy is indicated by a gray horizontal line, and the epochs at which bursts were detected in these observations at the VLA are identified by red triangles. (c) The spectrum of the PRS from VLA observations spanning 1–25 GHz. The integrated flux density is plotted for each epoch of observation and shows a spectrum inconsistent with a single power law. Abbreviations: FRB, fast radio burst; MJD, modified Julian day; PRS, persistent radio source; RMS, root-mean-square; VLA, Very Large Array.

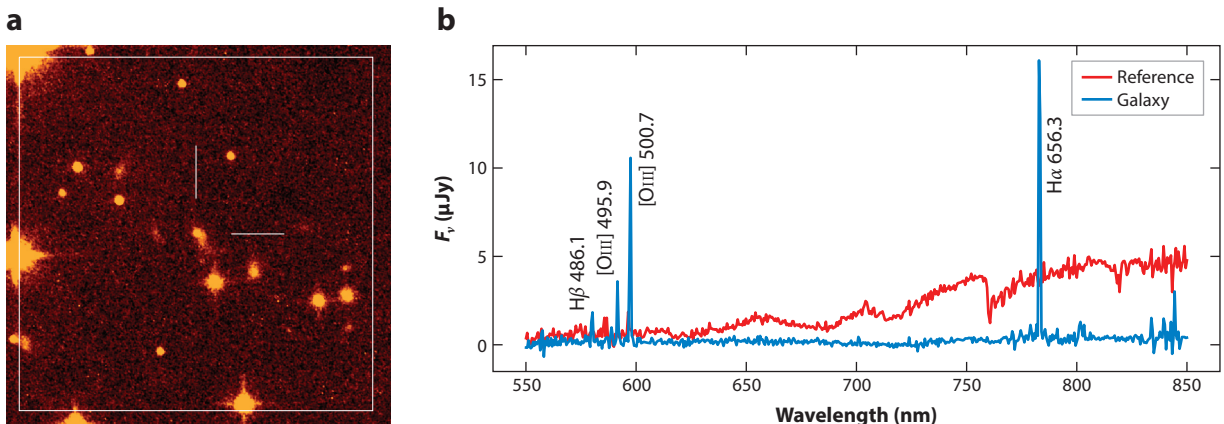


Figure 10

(a) Image from the HST/WFC3 in the F110W filter (equivalent to J-band) showing the resolved irregular dwarf galaxy host of FRB 121102 (Bassa et al. 2017). A prominent knot of star formation dominates the optical emission. Lines indicating North and East are 3 arcsec in length. (b) The spectra of the host galaxy and the reference object (Tendulkar et al. 2017). Prominent emission lines are identified and labeled with their rest-frame wavelengths in nanometers, demonstrating the redshift of the galaxy. Abbreviations: FRB, fast radio burst; HST, *Hubble Space Telescope*; WFC3, Wide Field Camera 3.

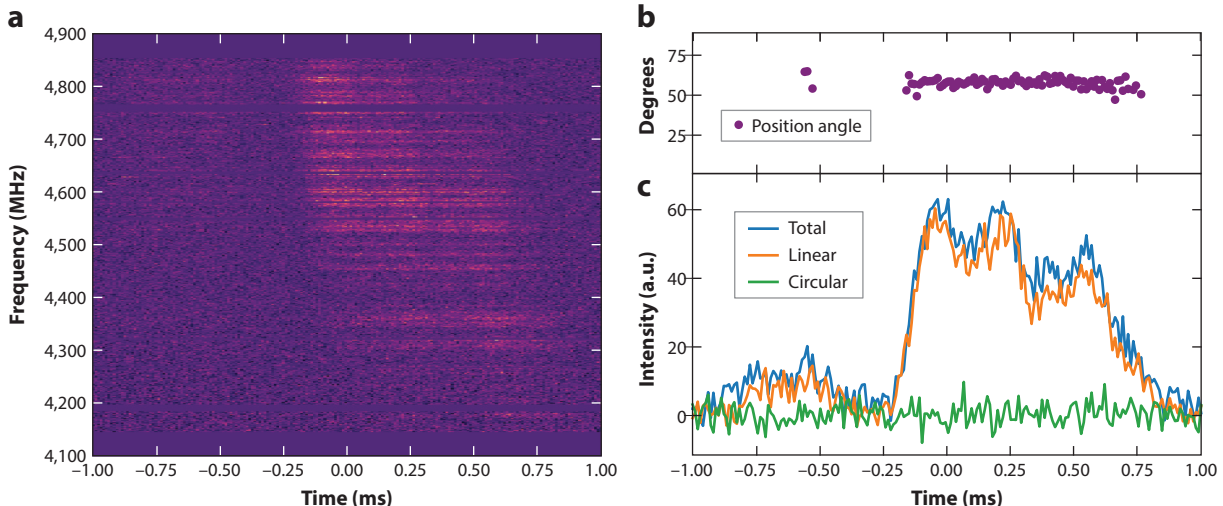


Figure 11

Dynamic spectrum, polarization angle, and pulse profile of a burst from FRB 121102 detected at Arecibo. (a) The burst dynamic spectrum, showing the fine structure in time and frequency. (b) The polarization position angle across the burst. (c) Total intensity (blue), linear polarization profile (orange), and circular polarization profile (green) for the burst. The burst is almost completely linearly polarized, with a constant polarization position angle. Figure based on observations by Michilli et al. (2018).

coherently dedispersed observations have enabled the detection of bursts from FRB 121102 at frequencies as high as 8 GHz (Law et al. 2017, Gajjar et al. 2018, Spitler et al. 2018), and revealed unexpected richness of time–frequency structure in the bursts (see, e.g., Figure 3).

Coherently dedispersed observations by Michilli et al. (2018) at Arecibo at 4.1–4.9 GHz also revealed that the bursts had nearly 100% linear polarization (Figure 11), and stacking of the bursts revealed a very high and variable rotation measure of $+1.46 \times 10^5$ to $+1.33 \times 10^5$ rad m $^{-2}$ over a seven-month period. Such a high rotation measure had previously only been observed in the environment of Sgr A* (Bower et al. 2003, Marrone et al. 2007), the supermassive BH in our GC. Furthermore, the large changes in the value of the RM without comparable changes in the burst DM require significant changes in the line-of-sight projected magnetic field. That rules out, for example, an HII region along the line of sight as the source of the high RM and implies that the source is embedded in an extreme magneto-ionic environment (Michilli et al. 2018). In what we suggest may not be a coincidence, such changes in RM without accompanying changes in DM have only been seen before for the GC magnetar J1745–2900 (Desvignes et al. 2018). The implications of the constraints from the DM, RM, and EM are discussed further below.

4.1. The Persistent Radio Counterpart Associated with FRB 121102

The nature of the PRS associated with FRB 121102 remains enigmatic. The source is compact and barely resolved with very long baseline observations, with a source size of 2–4 mas at 1.7 GHz and 0.2–0.4 mas at 5 GHz (Marcote et al. 2017). The radio spectrum of the source (Figure 9) is non-thermal and inconsistent with a single power law (Chatterjee et al. 2017), and the flux density at 2–4 GHz is variable on about day timescales, ranging between 190 ± 50 μ Jy over observations from 2016 to 2018 (Figure 9). Chatterjee et al. (2017) show that of the 69 sources detected within a 5-arcmin radius, 9 (including the PRS) show significant variability as defined by a reduced χ^2 metric ($\chi_r^2 > 5.0$), and that the variability is uncorrelated with the detection of bursts in the

uniform VLA data set (point biserial correlation coefficient $r = 0.054$, exceeded by chance 75% of the time).

Were it not for the knowledge that the PRS is associated with FRBs, we would readily conclude that it is consistent with a weak AGN. Indeed, given the inference of an extreme magneto-ionic environment associated with the burst source (Michilli et al. 2018), and its similarity to the GC magnetar J1745–2900, the AGN model remains an attractive explanation for the PRS. An alternative model presented by, e.g., Metzger et al. (2017) and Margalit & Metzger (2018) is that the PRS is a magnetized electron–ion nebula powered by the termination shock of a relativistic magnetar wind, which implicates a very young magnetar as the source of the bursts from FRB 121102.

4.2. Burst Periodicity and Sporadicity

Bursts from FRB 121102 have been detected with separations as small as 22.7 s (Arecibo, 1.4 GHz; Scholz et al. 2016), at an epoch when 6 bursts were detected in a contiguous 1,002-s observation. At the GBT at 4–8 GHz, Gajjar et al. (2018) have reported at least 18 bursts in a 1,800-s scan, with bursts as close together as 11.3 s, although there may be even smaller separations, depending on the threshold for believable bursts (Zhang et al. 2018). These detections have been searched for periodicity using Fourier techniques, fast-folding analyses, and brute force trials, with no significant detection of a period longer than 100 ms. Phase-coherent trials are not feasible over widely spaced epochs, and the false alarm probability is too high for periods much shorter than 100 ms. An underlying period (due to source rotation, say) could also be masked by an accelerated binary orbit, by a wide rotational phase window for the burst emission, or by plasma lensing effects that result in variable path lengths even for closely spaced bursts.

Meanwhile, the bursts are also sporadic in nature: As shown in **Figure 9**, comparable VLA observations led to no burst detections in the first 21 epochs (1 h each) in April–May, 2016, followed by the detection of 9 bursts over the next 16 epochs in August–September, 2016 (Chatterjee et al. 2017). With GBT observations, Gajjar et al. (2018) report 18 bursts in 30 min, 21 bursts in the first hour, and no further comparably bright detections in the remaining 4 h (although Zhang et al. 2018 report fainter bursts). Such sporadicity is consistent with time-variable focusing or lensing effects, and if such a situation holds for other FRB sources as well, there are severe implied difficulties in placing meaningful constraints on the absence of repeat bursts.

4.3. Scattering of FRB 121102

There is no evidence for extragalactic scattering (pulse broadening), even at the lowest frequency at which bursts have been detected (1.2 GHz). Early detections in the 1.2–1.6 GHz band also showed no scintillation structure from either Galactic or extragalactic scattering. However, higher-frequency observations (Gajjar et al. 2018, Spitler et al. 2018) and coherently dedispersed 1.4-GHz measurements reveal narrow scintillation structure. A multifrequency fit to the published data yields a frequency scaling $\Delta\nu_d \sim (7.5 \pm 0.3 \text{ kHz})\nu^{-4.0 \pm 0.15}$ that is consistent with plasma scattering and the prediction (within a factor of two) with the NE2001 model (Cordes & Lazio 2002). Similarly, the (deconvolved) angular diameters of the burst source and the PRS, $\theta_o \sim 2 \pm 1 \text{ mas}$ and $\theta_o \sim 2\text{--}4 \text{ mas}$ at 1.7 GHz, respectively (Marcote et al. 2017), are also consistent with Galactic scattering and the relation between angular and temporal broadening. The consistency with the NE2001 model contrasts with the YMW16 model (Yao et al. 2017), which does not model scattering explicitly but instead evaluates the scattering time τ using the empirical relation between τ and DM base on Galactic pulsars. This overpredicts the scattering by a factor of 30.

4.4. Constraints on the Magnetoionic Circumsource Medium

The measurements of DM and RM, the absence of detectable extragalactic scattering, and possible plasma lensing provide empirical constraints on the source environment. We attribute a nominal $\text{DM}_{\text{RM}} \lesssim 100 \text{ pc cm}^{-3}$ to the circumsource Faraday region. Using a nominal host-galaxy contribution $\text{RM}_h = 10^5 \text{ RM}_5 \text{ rad m}^{-2}$, the parallel magnetic field is $B_{\parallel}^{(\text{meas})} = 123 \text{ mG} \text{ RM}_5 \text{ DM}_{\text{RM}}$. Equating B_{\parallel} to that expected for a region of thickness l with plasma β (thermal to magnetic energy) and a geometric factor $\eta_B = B_{\parallel}/B \leq 1$, we obtain

$$\begin{aligned} n_e &= 4.2 \times 10^8 \text{ cm}^{-3} (\eta_B^2 T_4 / \beta)^{-1} \text{ RM}_5^2 \text{ DM}_{\text{RM}}^{-2}, \\ l &= 9.4 \times 10^{-4} \text{ AU} (\eta_B^2 T_4 / \beta)^{-1} \text{ RM}_5^{-2} \text{ DM}_{\text{RM}}^3, \\ \text{EM} &= n_e^2 l = n_e \times \text{DM}_{\text{RM}} = 2.2 \times 10^8 \text{ pc cm}^{-6} (\eta_B^2 T_4 / \beta)^{-1} \text{ RM}_5^2 \text{ DM}_{\text{RM}}^{-1}. \end{aligned} \quad 10.$$

The free-free optical depth through the region is (Draine 2011, his equation 10.22 with ν in gigahertz)

$$\tau_{\text{ff}} = 3.37 \times 10^{-7} T_4^{-1.3} \nu^{-2.1} \text{EM} = 71 T_4^{-1.3} \nu^{-2.1} (\eta_B^2 T_4 / \beta)^{-1} \text{ RM}_5^2 \text{ DM}_{\text{RM}}^{-1}. \quad 11.$$

A small optical depth $\tau_{\text{ff}} \ll 1$ at 1 GHz requires the composite gas factor $\eta_B^2 T_4 / \beta \gg 1$, which increases the depth l . If plasma lensing occurs for a transverse lens scale a , requiring the focal distance $d_f \lesssim 1 \text{ GHz}$ at a frequency ν_I (Section 3.4.4), defining the depth to be a multiple A of a , $l = Aa$, and using d_{sl} in parsecs, d_{so} in gigaparsecs,

$$\begin{aligned} l &\leq 2.5 \text{ AU} (d_{\text{sl}} d_{\text{so}})^{1/2} \text{ DM}_{\text{RM}}^{1/2} (A/\nu_I), \\ \left(\frac{\eta_B^2 T_4}{\beta} \right) &\leq 2.6 \times 10^3 \text{ RM}_5^2 \text{ DM}_{\text{RM}}^{-5/2} (A/\nu_I) (d_{\text{sl}} d_{\text{so}})^{1/2}, \\ n_e &\geq 8.42 \times 10^4 \text{ cm}^{-3} (d_{\text{so}} d_{\text{sl}})^{-1/2} \text{ DM}_{\text{RM}}^{1/2} (A/\nu_I)^{-1}, \\ \text{EM} &\geq 8.42 \times 10^4 \text{ pc cm}^{-6} (d_{\text{so}} d_{\text{sl}})^{-1/2} \text{ DM}_{\text{RM}}^{3/2} (A/\nu_I)^{-1}, \\ \tau_{\text{ff}} &\geq 0.028 T_4^{-1.3} \nu^{-2.1} (d_{\text{so}} d_{\text{sl}})^{-1/2} \text{ DM}_{\text{RM}}^{3/2} (A/\nu_I)^{-1}. \end{aligned} \quad 12.$$

The situation may be more complex, of course, with distinct Faraday and lensing regions, for example. However, there is sufficient latitude to account for the measured Faraday rotation as well as the lensing requirements. For a small $\text{DM}_{\text{RM}} = 1 \text{ pc cm}^{-3}$, the Faraday region is very thin ($l \lesssim 1\text{--}10 \text{ AU}$), highly magnetized ($B \gtrsim 1 \text{ G}$), and dense ($n_e \gtrsim 10^5 \text{ cm}^{-3}$). The optical depth then need not be large, $\tau_{\text{ff}} \gtrsim 0.03$ at 1 GHz, but will be optically thick at frequencies no lower than about 100 MHz.

5. HOST GALAXIES AND COUNTERPARTS

The identification of host galaxies is a key step to obtaining FRB distances and energetics, and to identifying the progenitor population. Efforts have included mapping of the beam shape to identify plausible sky regions and candidate hosts based on multibeam detections (Ravi et al. 2016), as well as the misidentification of a variable radio source as an afterglow (Keane et al. 2016). As pointed out by Williams & Berger (2016), Vedantham et al. (2016b), and others, radio variability is commonplace and cannot be relied on as a sole indicator for an FRB host galaxy. However, the PRS associated with FRB 121102 is variable, along with several other sources in

the field (Section 4.1), and selecting luminous radio sources associated with galactic disks, after excluding AGN and background sources, may offer a reasonable sample for a targeted FRB search (Ofek 2017). Rapid multiwavelength follow-up to detect the analog of GRB afterglows has not been fruitful either (e.g., Petroff et al. 2017a, Tominaga et al. 2018), and the absence of high-energy emission associated with FRB 121102 (Scholz et al. 2017) makes such routes less promising for host identification. At present, therefore, the only reliable method demonstrated is the direct interferometric localization of the burst itself. Eftekhari & Berger (2017) show that \sim 1-arcsec localizations are required for unique host-galaxy identifications, although if all FRBs are associated with PRSs like FRB 121102, Eftekhari et al. (2018) show that the localization requirements are much less stringent, at the 10-arcsec level.

The one uniquely identified host galaxy for FRB 121102 is an irregular low-metallicity star-forming dwarf with a strong resemblance to the hosts of long-duration GRBs and SLSNe (Section 4), leading to a unified model for the source of the repeating bursts and the PRS as a young millisecond magnetar embedded in a nebula powered by its relativistic wind (Metzger et al. 2017, Margalit & Metzger 2018). If most FRBs come from repeating sources, Nicholl et al. (2017) find that a source association with GRBs or SLSNe and a burst emission lifetime of 30–300 years makes for a self-consistent picture. Although such a model has many attractive features, the PRS does resemble a typical AGN, and it has been established that dwarf galaxies can have massive BHs (Reines et al. 2011, Seth et al. 2014). The high (and time-varying) RM of the bursts, without a correspondingly large change in DM, argues for an extreme magneto-ionic environment similar to that of our GC (Michilli et al. 2018). Of course, one could require both circumstances (a very young magnetar in the environment of a massive BH) for (repeating) FRBs, a proposition difficult to rule out given a sample of one (as of February 2019).

Even in the absence of a specific host-galaxy identification, the very low DM of FRB 171020 (114 pc cm^{-3} ; Shannon et al. 2018) leads to a very restrictive upper limit on the distance to a host, and Mahony et al. (2018) identify ESO 601–G036, an Sc galaxy at a redshift $z \sim 0.009$, as the most plausible host galaxy. However, the candidate host is not associated with a PRS, nor is there a candidate PRS within $z \lesssim 0.06$, suggesting that it may not be a generic feature for (all classes of) FRB emission. We discuss possible central engine models further below; further host identifications are the most urgent observational priority for FRB science.

6. SURVEYS AND POPULATIONS

6.1. The Fluence–DM Distribution

Measured FRB fluences \mathcal{F} are lower bounds in many cases (currently) due to uncertainties in location within telescope beams, but they also show the wide range expected from a spatially distributed population having a wide intrinsic luminosity function.⁷ If the extragalactic portion of the dispersion measure $\text{DM}_x = \text{DM} - \widehat{\text{DM}}_{\text{MW}}$ is a proxy for distance, the distribution of \mathcal{F} versus DM_x should provide some insights.

Figure 12 shows this distribution for FRBs detected in the \sim 1.4-GHz band from the Arecibo, ASKAP, and Parkes surveys (along with other FRBs). Broad conclusions that can be made include the following:

- The ASKAP and Parkes surveys yield fluences that are largely independent of DM_x .

⁷Also, beamed radiation introduces the unknown angle between the beam axis and the line of sight that further increases the range of apparent luminosities.

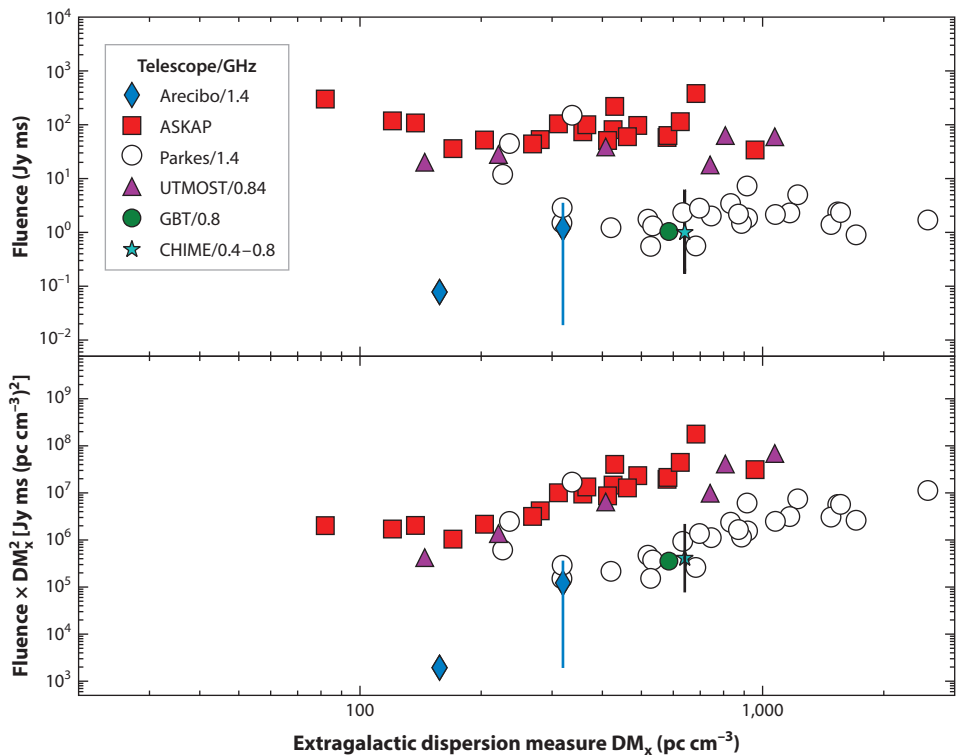


Figure 12

Fluence versus estimated extragalactic dispersion measure, DM_x for FRB discoveries reported in FRBCAT and Shannon et al. (2018). The CHIME FRB 180725A has no reported fluence but the vertical line (black) represents the plausible range of values. The blue line represents the range of values for the repeating FRB 121102. Abbreviations: ASKAP, Australian Square Kilometre Array Pathfinder; CHIME, Canadian Hydrogen Intensity Mapping Experiment; DM, dispersion measure; FRBCAT, Fast Radio Burst Catalog; GBT, Green Bank Telescope; UTMOST, the updated Molonglo Observatory Synthesis Telescope.

- The mean $\langle \mathcal{F} \rangle$ is larger for ASKAP than Parkes by a factor of ~ 30 , which is of order the sensitivity ratio of the 64-m Parkes telescope and ASKAP’s 12-m antennas (for the fly’s eye mode used by Shannon et al. 2018).
- The scatter in fluence $\sigma_{\log \mathcal{F}} \lesssim 0.5$ for the two surveys.
- The repeating FRB 121102 by itself shows a large scatter (by 10^2) between burst amplitudes, indicating intrinsic variance that is not unlike that seen from individual pulses of pulsars.

A simple analysis is instructive for estimating some rough numbers. The (pseudo) luminosity $\mathcal{L} = S_{\text{pk}} d_{\text{so}}^2$ defined earlier is $\mathcal{L} \sim (\mathcal{F}/W)d_{\text{so}}^2 \propto (\mathcal{F}/W)DM_x^2$ if DM_x is a proxy for the source–observer distance d_{so} . This gives $\mathcal{F} \propto \mathcal{L}W/DM_x^2$. We show $\mathcal{F}DM_x^2$ in **Figure 12**. Standard candles and a constant width would imply $\mathcal{F}DM_x^2 = \text{constant}$, whereas scatter in \mathcal{L} and W implies vertical scatter in the \mathcal{F} – DM_x distribution. Cosmic variance and errors in estimating DM_x give horizontal scatter that combines with the variations of the true extragalactic DM. The clear difference in average $\mathcal{F}DM_x^2$ for the ASKAP and Parkes samples demonstrates vividly that FRBs are not standard candles, as pointed out by Shannon et al. (2018). Only a subset of the Parkes FRBs shown in the figure come from the uniform set of surveys listed in **Table 1**. These are the events with

$\text{DM}_x > 400 \text{ pc cm}^{-3}$. For this subset, $\langle \log \text{DM}_x \rangle \sim 2.9$ compared to 2.5 for the ASKAP sample. The corresponding fluences have $\langle \log F \rangle \sim 0.4$ and 1.9, respectively.

The systematic rise in $\mathcal{F}\text{DM}_x^2$ scales roughly as DM_x^2 for both the ASKAP and Parkes samples and is to be expected for threshold-limited surveys. However, scatter about this trend is also expected when there are significant host-galaxy contributions to DM_x . The apparent flattening (beware small number statistics!) for $\text{DM}_x \leq 200 \text{ pc cm}^{-3}$ may result from host-galaxy DMs.

It is also instructive to compare the number of burst detections in the ASKAP and Parkes surveys. Let $d_1 = (3/\eta_1 n_s \Omega_s T)^{1/2}$ be the distance out to which only a single burst event is expected for an exposure time T per sky position, where η_1 is the burst rate per source and n_s is the number density of sources. The number of events occurring out to an arbitrary distance d is $N_e(d) = (d/d_1)^3$. Only a fraction of these events is detectable. Assume that burst detection corresponds to peak flux densities exceeding a threshold S_{\min} .

The detection number is $N_d(d_L) = (d_L/d_1)^3$, where d_L is the maximum distance that a burst with luminosity \mathcal{L} could be detected. Noting that both d_L and d_1 are survey dependent, the ratio of the ASKAP to Parkes survey yields is (using values in **Table 1**)

$$\frac{N_d(\text{A})}{N_d(\text{P})} = \left[\frac{d_L(\text{A})}{d_L(\text{P})} \right]^3 \left[\frac{d_1(\text{P})}{d_1(\text{A})} \right]^3 = \left(\frac{\mathcal{F}_{\min,\text{P}}}{\mathcal{F}_{\min,\text{A}}} \right)^{3/2} \frac{(\Omega_s T)_\text{A}}{(\Omega_s T)_\text{P}} \approx 2. \quad 13.$$

By comparison, the actual numbers are in the ratio $N_d(\text{A})/N_d(\text{P}) \sim 1.1$. Clearly, the wider field and longer dwell time T for the ASKAP survey more than compensate for the sensitivity difference.

6.2. Some Population Numbers

A simple analysis of the events in **Figure 12** illustrates some constraints that can be made on the event rate density $\dot{n}_s = \eta_1 n_s$. We assume that the lowest DM_x FRB in a survey is also at the lowest distance \hat{d} with $d_1 \lesssim \hat{d}$, which constrains d_1 , the distance out to which only one burst occurs in a survey. Using the mean IGM electron density n_{e_0} to estimate \hat{d} and knowing the survey parameter $\Omega_s T$ (**Table 1**), the likelihood function for \dot{n}_s is $\mathcal{L}(\dot{n}_s) = (\dot{n}_s/\langle \dot{n}_s \rangle) \exp -\dot{n}_s/\langle \dot{n}_s \rangle$, where

$$\langle \dot{n}_s \rangle = \frac{3}{\Omega_s T d_1^3} \gtrsim \frac{3}{\Omega_s T \hat{d}^3} \sim \begin{cases} 112 \text{ events Gpc}^{-3} \text{ d}^{-1} & \text{ASKAP survey} \\ 97 \text{ events Gpc}^{-3} \text{ d}^{-1} & \text{Parkes survey.} \end{cases} \quad 14.$$

The source number density n_s is not known empirically but has been estimated by Nicholl et al. (2017) as $n_s \approx 10^4 \text{ Gpc}^{-3}$ for dwarf galaxies that harbor SLSNe. Combining this with $\dot{n}_s \approx 100 \text{ Gpc}^{-3} \text{ d}^{-1}$, we obtain the mean burst rate per source $\eta_1 \approx 10^{-2} \text{ d}^{-1}$. This average rate is exceeded by a large factor by the repeater FRB 121102 at some epochs but may be consistent with overall average FRB detection statistics.

6.3. Modulated Luminosity Functions and Detection Numbers

We now consider the effects of scintillations and lensing on FRB detection rates. We assume that all individual FRB sources emit bursts according to the same luminosity distribution $f_L(\mathcal{L})$. The overall population luminosity function is the combination of individual luminosity distributions weighted by the number of sources per unit volume. Our analysis is primarily in Euclidean space, and we extend to cosmological contexts as needed. A more detailed analysis will be published elsewhere. Cosmological effects are discussed by Cordes & Wasserman (2016) and Macquart & Ekers (2018a).

The number of detections in the absence of propagation effects is

$$N_d(d) = \frac{3}{d_1^3} \int_0^d dD D^2 \int_{S_{\min} D^2}^{\infty} d\mathcal{L} f_L(\mathcal{L}). \quad 15.$$

With scintillations or lensing (or absorption) characterized with a PDF $f_g(g)$, the modified number of detections is

$$N_{dg}(d) = \frac{3}{d_1^3} \int dg f_g(g) \int_0^d dD D^2 \int_{S_{\min} D^2/g}^{\infty} d\mathcal{L} f_L(\mathcal{L}). \quad 16.$$

By inspection, for a fixed gain $g(v, t)$, a modulation $g > 1$ effectively lowers the threshold to S_{\min}/g or it effectively increases luminosities to $\sqrt{g}\mathcal{L}$. When g varies over an ensemble of events with unit mean (appropriate for scintillation and lensing), some nearby events become undetectable while other more distant events become detectable.

6.3.1. Standard candles and power-law luminosities. A toy model comprising standard candles illustrates salient points that also apply to more realistic luminosity functions. Using $f_L(\mathcal{L}) = L_0 \delta(\mathcal{L} - L_0)$, the maximum detection distance is $d_{L_0} = \sqrt{L_0/S_{\min}}$. **Figure 13** shows survey volumes for two cases, one in which the detection distance exceeds d_1 and the other in which no sources can be detected without lensing or DISS. The differential detection number is nonzero only for $D \leq d_{L_0}$:

$$\frac{dN_d}{dd} = \frac{3D^2}{d_1^3} \Theta(d_{L_0} - D), \quad 17.$$

and its ratio to the differential number of events dN_e/dd is

$$\frac{dN_d/dd}{dN_e/dd} = \Theta(d_{L_0} - D). \quad 18.$$

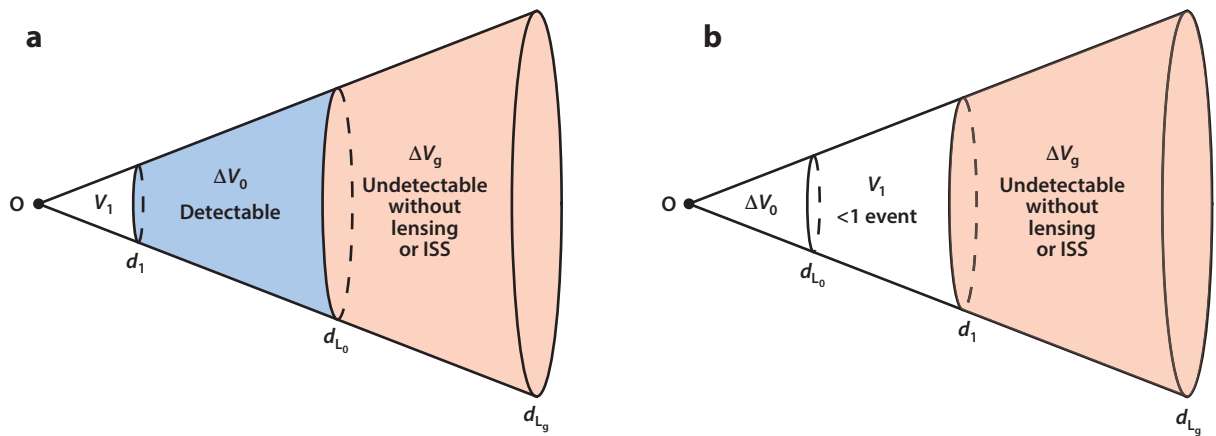


Figure 13

Survey volumes for standard candles. Only one burst occurs within d_1 , on average; d_{L_0} is the maximum detectable distance without scintillations; and d_{L_g} is the maximum distance when scintillations occur, $d_{L_0} > d_1$. (a) The case in which bursts are bright enough to detect without any lensing or scintillation boost, $d_1 > d_{L_0}$. Lensing or scintillations are required for burst detections. Abbreviation: ISS, interstellar scintillation.

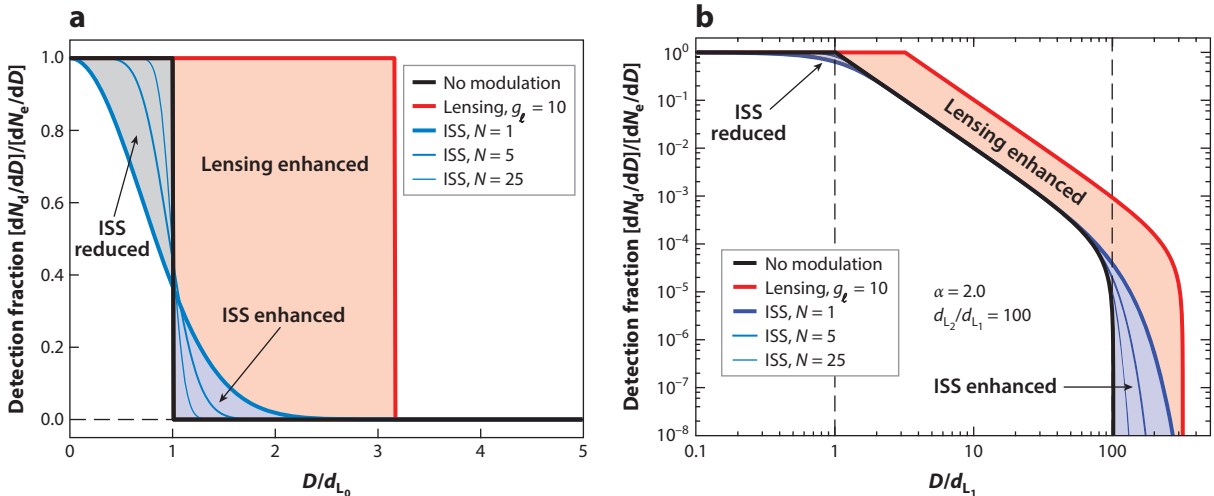


Figure 14

(a) Differential fraction of events detected for standard candles with and without DISS or lensing. The abscissa is the distance in units of d_{L_0} , the maximum detection distance in the absence of an extrinsic gain. ISS curves for three RMS values $\sigma_g = N^{-1/2}$ are shown (where N is the number of summed, independent “scintles”), and the example lens gain is $g_\ell = 10$. (b) Differential fraction of detections for events with a power-law luminosity function with and without ISS or lensing. The abscissa is the distance in units of d_{L_1} , the maximum detection distance of the weakest bursts in the absence of an extrinsic gain. The corresponding distance for the strongest bursts is d_{L_2} . Abbreviations: DISS, diffractive interstellar scintillation; ISS, interstellar scintillation; RMS, root mean square.

All events from distances smaller than d_{L_0} but none for larger distances, are detected. Inclusion of a constant lens gain g_ℓ in a standard lensing model increases the detection distance to $\sqrt{g_\ell} d_{L_0}$ and the total number of detected events from $(d_{L_0}/d_1)^3$ to $g_\ell^{3/2} (d_{L_0}/d_1)^3$.

If the burst rate density $\dot{n}_s = \eta_1 n_s$ is large enough so that $d_1 < d_{L_0}$, some bursts will be detected without any lensing boost, but the total number will dramatically increase with $g_\ell \gg 1$. Episodes of lens dimming ($g_\ell < 1$) reduce the number. In the opposite case of a sparse rate density, detections require strong lensing. **Figure 14** shows the differential ratio from Equation 18 for standard candles (**Figure 14a**) and for a power-law case (**Figure 14b**), with regions indicated where detection numbers are enhanced or diminished by scintillations of lensing.

With scintillations included, the number of detections becomes

$$N_{dg}(d) = \frac{d^3 \Gamma[N, N(d/d_{L_0})^2] + d_{L_0}^3 \gamma[N + 3/2, N(d/d_{L_0})^2]}{d_1^3 \Gamma(N)}, \quad 19.$$

where $\Gamma(a, b)$ and $\gamma(a, b)$ are the incomplete gamma functions. For fully modulated DISS with $N = 1$, $f_g(g) = e^{-g}\Theta(g)$, and the number of detections at distances nearer than d_{L_0} is reduced to $\Gamma(1, 1) + \gamma(5/2, 1) \sim 0.57$ of the original number because of scintillations $g < 1$, but now a larger total number is detected, $N_{dg}(\infty) = \Gamma(5/2)N_e(d_{L_0}) \sim 1.33N_e(d_{L_0})$, owing to scintillation boosts of sources beyond d_{L_0} .

7. THE FRB DISTANCE SCALE

Measurement of the redshift of a securely associated galaxy is the only reliable method for determining FRB distances, and that is likely to remain the case. Repeated bursts from the source of FRB 121102 were key to enabling its subarcsecond localization that led to the redshift of the dwarf host galaxy. Absent a radio localization from the first (and perhaps only) burst from an FRB

source, host-galaxy associations are likely only for nearby, low-DM FRBs in which a small number of galaxies is in the positional error box. For most bursts, which tend to be one-offs or at least very infrequent repeaters, localizations need to be done at the time of discovery using interferometric arrays. Until such arrays operate routinely, approximate distance estimates will be obtained from DMs. Here, we summarize DM-based methods and their issues.

It is useful to consider the total DM and pulse broadening time together. Measured values include contributions from the host, the IGM (including cosmic variance), and the MW along with other contributions that can arise from the circumsource environment, intervening galaxies, galaxy clusters, or unmodeled HII regions in the MW,

$$\text{DM}_{\text{frb}} = \text{DM}_h + \text{DM}_{\text{IGM}} + \text{DM}_{\text{MW}} + \text{DM}_{\text{other}} \quad 20.$$

$$\tau_{\text{frb}} = \tau_h + \tau_{\text{IGM}} + \tau_{\text{MW}} + \tau_{\text{other}}. \quad 21.$$

7.1. Deconstructing Dispersion Measure

The general approach so far has been to estimate the IGM's contribution by subtracting estimates for the host galaxy and the MW while ignoring other terms,

$$\widehat{\text{DM}}_{\text{IGM}} = \text{DM}_{\text{frb}} - \widehat{\text{DM}}_{\text{host}} - \widehat{\text{DM}}_{\text{MW}}. \quad 22.$$

Estimates for the MW term come from the NE2001 and YMW16 models and inclusion of a Galactic halo contribution $\text{DM}_{\text{halo}} \approx 30 \text{ pc cm}^{-3}$. Host-galaxy contributions are often fixed to low constant values such as $\sim 50 \text{ pc cm}^{-3}$ (Shannon et al. 2018) or $\sim 100 \text{ pc cm}^{-3}$ based on the (questionable) assumption that the host contributions arise solely from MW-type ISMs averaged over inclination angles. Although MW models have systematic errors due to unmodeled HII regions (interstellar variance), the uncertainties in $\widehat{\text{DM}}_{\text{MW}}$ are probably smaller than typical host-galaxy contributions, particularly for high-latitude FRBs.

The only empirical constraint on host-galaxy contributions comes from the repeating FRB for which Balmer-line-based estimates of the EM translate into $\widehat{\text{DM}}_{\text{host}} \approx 100\text{--}200 \text{ pc cm}^{-3}$. The assumption of generally small host-galaxy contributions runs counter to FRB models involving young SNe (Piro 2016), whose expanding shock fronts imply very large DM values that can hinder detection of bursts at early times, or models involving AGNs (e.g., Zhang 2017) in the centers of galaxies. Without other constraints, it must be allowed that a circumsource contribution could be a large fraction of the DM for even the largest measured $\text{DM}_{\text{frb}} = 2,596 \text{ pc cm}^{-3}$ (FRB 160102). Consequently, the error on any given estimate for $\widehat{\text{DM}}_{\text{IGM}}$ may be very large.

7.2. Dispersion Measure–Redshift Relation

Reionization at $z \gtrsim 10$ has rendered most of the baryons in the Universe to a largely invisible status in the IGM, often referred to as the missing baryons (Nicastro et al. 2018). Measurements that constrain the IGM are therefore valuable for understanding the distribution and temperature-density phase structure of the ionized gas. Future FRBs may provide much of that information once host-galaxy redshifts are measured routinely in large numbers and host-galaxy contributions are better estimated. For now, IGM considerations have largely concerned the reciprocal problem of using $\widehat{\text{DM}}_{\text{IGM}}$ to estimate the redshifts of FRBs. Published analyses of the DM- z relation that conclude dominance by the IGM border on the procrustean because they attribute rather small values of the host-galaxy contribution DM_h in the absence of any direct measurement (other than for FRB 121102). Assumption of small DM_h runs counter to viable models involving young neutron stars (NSs), where significant circumsource contributions to DM are expected.

Invariance of the electromagnetic phase, $\phi = -\lambda r_e \int_0^D ds n_e(s)$ (Jackson 1962), implies

$$DM(d_{so}) = \int_0^{d_{so}} \frac{d\ell n_e(\ell)}{(1+z)}.$$

For a galaxy at redshift z_g with dispersion measure DM_g , an observer measures $DM(z_g) = DM_g/(1+z_g)$, whereas an arbitrary distribution of n_e gives

$$DM(z_s) = \frac{c}{H_0} \int_0^{z_s} \frac{dz n_e(z)}{(1+z)^2 E(z)}, \quad 23.$$

where in flat Λ CDM spacetime $E(z) = \sqrt{\Omega_m(1+z)^3 + 1 - \Omega_m}$. For the IGM, $n_e(z) = n_{e0}(1+z)^3 \mu_e/\mu_{e0}$, where $\mu_e/\mu_{e0} \sim 1$ expresses the degree of ionization of hydrogen and helium, and the local ($z=0$) mean electron density $n_{e0} = \mu_{e0} \Omega_{GM} \rho_c/m_p$ yields the mean DM,

$$\overline{DM}_{IGM}(z_s) = \frac{cn_{e0}}{H_0} \int_0^{z_s} dz \frac{(1+z)}{E(z)} \frac{\mu_e}{\mu_{e0}}. \quad 24.$$

We use the Planck 2015 cosmological parameters ($H_0 = 67.7 \text{ km s}^{-1} \text{ Mpc}^{-1}$, $\Omega_{m0} = 0.307$, and $\Omega_{b0} = 0.0486$) to obtain $n_{e0} \sim 2.2 \times 10^{-7} \text{ pc}^{-3}$ and evaluate the fiducial dispersion measure, $DM_f = cn_{e0}/H_0 = 977 \text{ pc cm}^{-3} (\Omega_{IGM}/\Omega_b)(\mu_e/\mu_{e0})$.

Cosmic variance yields significant variations about the mean from \overline{DM}_{IGM} that are estimated from cosmological simulations by several authors and expressed in the form of a standard deviation versus redshift, $\sigma_{DM}(z)$. The fractional RMS $\sigma_{DM}(z)/\overline{DM}_{IGM}(z)$ decreases with larger z but fairly slowly. Consolidating the results of Ioka (2003), Inoue (2004), McQuinn (2014), Dolag et al. (2015), and Shull & Danforth (2018), we show DM(z) in **Figure 15**. For fixed z the DM distribution is asymmetric with large positive excursions expected when the line of sight intersects dense halos (rich galaxy clusters) or individual galaxies for $z_s \gg 1$, as noted by Dolag et al. (2015). Intersections with massive halos become highly probable for $z > 1$ (Voit et al. 2001, McQuinn 2014, Cordes & Wasserman 2016), so redshifts derived from FRBs with large DMs must be regarded with suspicion if intersections are ignored. Future analysis can look for correlations of large FRB DMs with proximity to galaxy clusters as both the FRB sample and cluster catalog increase in size. If DMs are IGM dominated, such a correlation should be found; conversely, the absence of a correlation is expected if FRBs are typically at $z_s < 1$ and DMs receive large host-galaxy contributions.

In addition to cosmic variance, errors in \widehat{DM}_{IGM} due to uncertainties in $\delta\widehat{DM}_{MW}$ and $\delta\widehat{DM}_{host}$ in the Galactic and host-galaxy contributions compound the difficulty of estimating redshifts. The resulting $\delta\widehat{DM}_{IGM} = \delta\widehat{DM}_{MW} + \delta\widehat{DM}_{host}$ implies [using $\bar{z}(DM)$ as the inverse of $\overline{DM}_{IGM}(z)$ and using δDM_{IGM}^{cv} to denote cosmic variance in the DM- z relation],

$$\widehat{z}(\widehat{DM}_{IGM}) = \bar{z}(DM_{IGM}) + \frac{d\bar{z}}{d\overline{DM}_{IGM}} \left(\delta DM_{IGM}^{cv} - \delta\widehat{DM}_{MW} - \delta\widehat{DM}_{host} \right). \quad 25.$$

MW contributions are estimated using Galactic electron density models, such as NE2001 (Cordes & Lazio 2002) and YMW16 (Yao et al. 2017), which have inherent errors due to complex Galactic structure that is not well modeled.

From **Figure 15**, $d\bar{z}/d\overline{DM}_{IGM} \approx 10^{-3}$, so each 100 pc cm^{-3} of error on \widehat{DM}_{IGM} gives $\delta z = 0.1$. What errors on \widehat{DM}_{IGM} can be expected? Differences between the NE2001 and YMW16 models at low Galactic latitudes suggest RMS $\delta\widehat{DM}_{MW}$ values exceeding 100 pc cm^{-3} (Tendulkar et al. 2017, Spitler et al. 2018), but high latitudes have errors a factor of 5 to 10 smaller. \widehat{DM}_{host} for the repeating FRB likely exceeds 100 pc cm^{-3} , and some authors argue that host-galaxy contributions will be no larger than this based on the notion that the host-galaxy contribution comes from

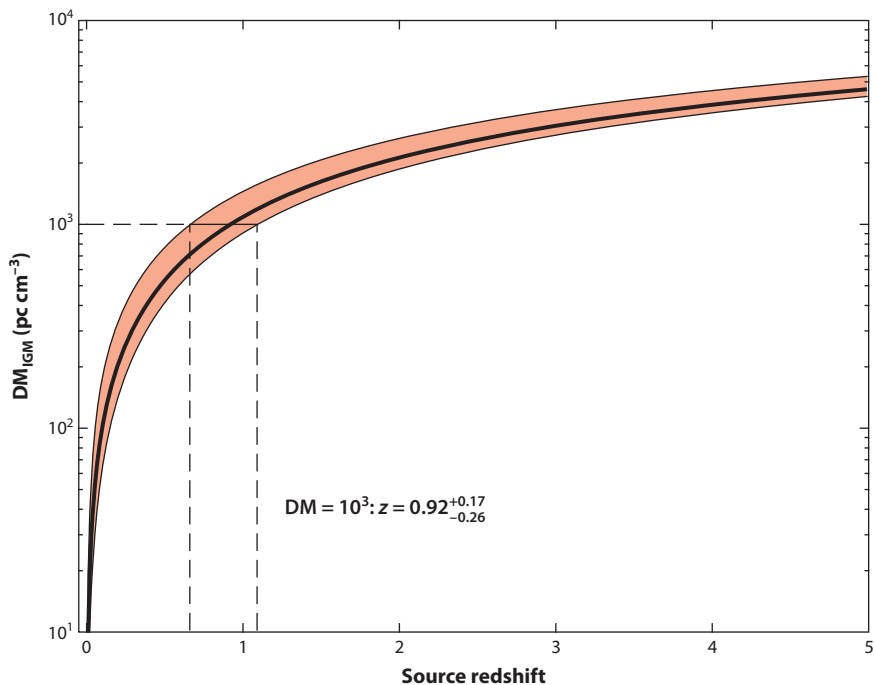


Figure 15

IGM contribution to DM versus redshift showing the average relation from Equation 24 (*thick black line*) and IGM dispersion measure based on cosmological simulation results characterized by Ioka (2003), Inoue (2004), McQuinn (2014), and Dolag et al. (2015). The range of z for $\text{DM}_{\text{IGM}} = 10^3 \text{ pc cm}^{-3}$ is indicated. Abbreviations: DM, dispersion measure; IGM, intergalactic medium.

a galaxy disk. However, FRBs may generally be embedded in star-forming regions, in galactic centers, or in a circumsource nebula that can provide much larger values. Consequently, redshift errors may be several tenths or more for $z \sim 1$.

7.3. The τ -Dispersion Measure Relation

Lines of sight to FRBs span plasmas with radically different properties, including the ISM, the IGM, the host galaxy's ISM, and the circumsource medium (contributions from the interplanetary medium and ionosphere are minor for FRB studies).⁸ Turbulence will differ greatly between them just as it does between intra-Galactic components.

To assess whether extragalactic scattering stems from the IGM or host galaxies, we compare the τ -DM relation for Galactic pulsars with FRB scattering in **Figure 16**. For a fixed DM, Galactic pulsars show more than an order of magnitude of variation in τ . **Figure 16a** shows the fit to the data of the empirical model, $\hat{\tau}(\text{DM}) = 2.98 \times 10^{-7} \text{ ms} \times \text{DM}^{1.4}(1 + 3.55 \times 10^{-5} \text{ DM}^{3.1})$ (Ramachandran et al. 1997), with roughly 5% errors on each parameter and a spread $\sigma_{\log \tau} = 0.76$ about the mean [data and fit in Cordes et al. (2016); update in preparation]. Values for FRB broadening time measurements as well as upper limits are shown in the figure. When measurable, FRB scattering is comparable with burst widths but clearly is biased below the pulsar band.

⁸We note, however, that any FRBs discovered in directions close to the Sun will likely be affected by interplanetary scintillation.

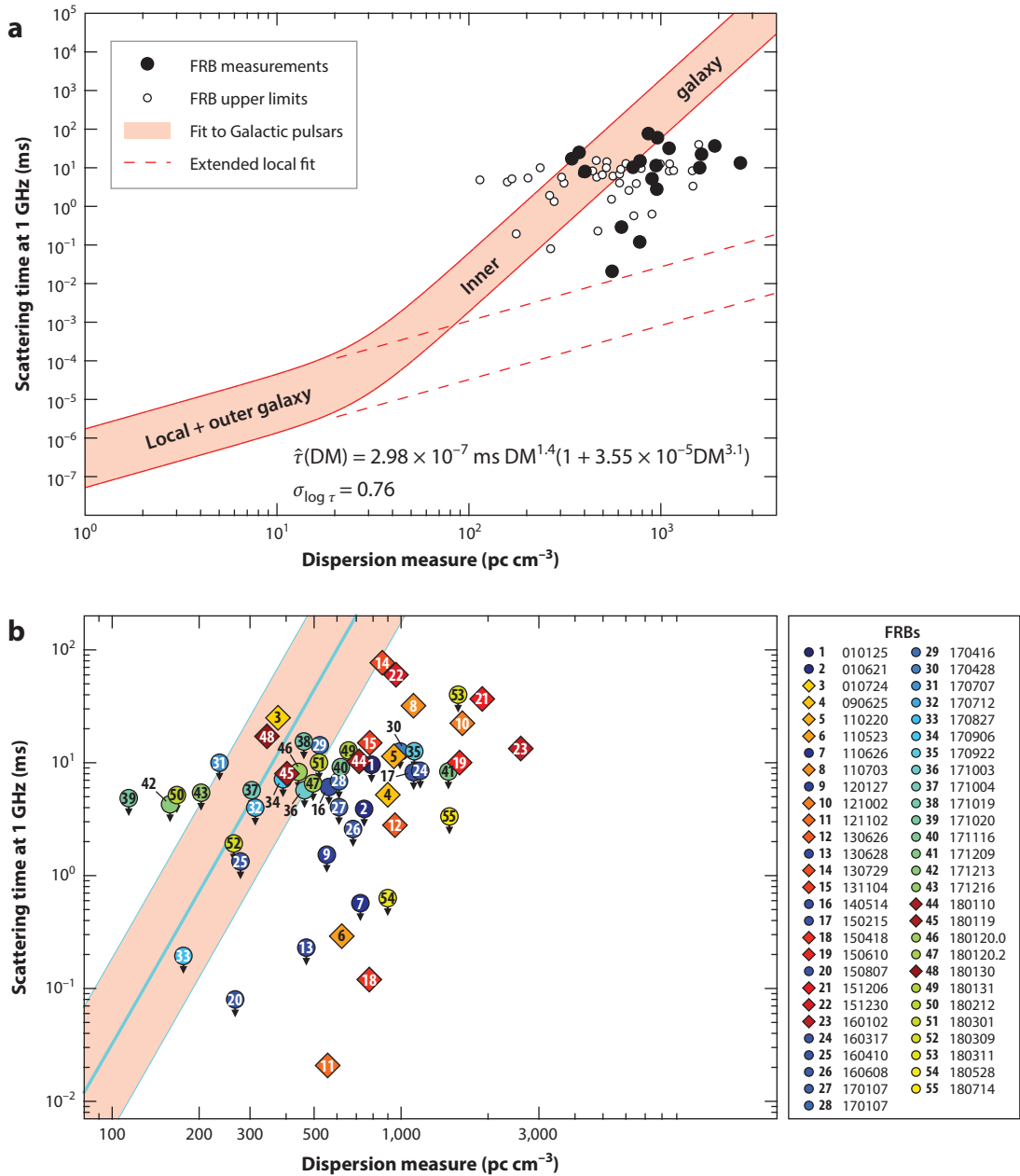


Figure 16

(a) Scattering times τ versus DM for pulsars and FRBs. Pulsar scattering is depicted as a shaded region described by the shown equation. FRB measurements are shown as filled circles and upper limits as open circles. Dashed lines extend the small-DM portion of the pulsar fit. (b) Zoom-in of the FRB region of τ -DM space using estimates of DM_x , the extragalactic dispersion measure, and with the Galactic scaling law based on pulsars shifted upward by 3 \times to account for plane wave geometry. Abbreviation: DM, dispersion measure; FRB, fast radio burst.

To interpret FRB scattering, the extreme heterogeneity of the mean scattering strength per unit DM needs to be accounted for. Galactic pulsars at large DMs sample the inner Galaxy in the spiral-arm and thin-disk components of the NE2001 electron density model. Scattering per unit length is significantly larger in those regions than in the outer Galaxy or in the thick disk component, thus causing the larger slope of the τ –DM distribution in **Figure 16a** for $DM \gtrsim 50 \text{ pc cm}^{-3}$. FRBs have been seen mostly at high Galactic latitudes and in the Galactic anticenter direction, which sample the more weakly scattering gas also indicated in the figure. The measured scattering of FRBs must be extragalactic in origin, as demonstrated in **Figure 4** of this review. However, for the corresponding DMs, the scattering is weaker than it would be for lines of sight through the disk of the Milky Way.

However, the scattering must be compared with only the extragalactic component of DM, which has contributions from the IGM and the host galaxy in a ratio that is unique to each FRB. We define the extragalactic contribution to DM as $DM_x = DM_{\text{frb}} - DM_{\text{MW}}$, where the estimated Galactic contribution $\bar{DM}_{\text{MW}} = DM_{\text{NE2001}}(l, b) + DM_{\text{halo}}$ is the sum of the NE2001 model integrated to its edge and a halo contribution, taken as a uniform value $DM_{\text{halo}} = 30 \text{ pc cm}^{-3}$ (Dolag et al. 2015). Similarly, we write $\tau_x = \tau_{\text{frb}} - \tau_G$, where we exclude a halo contribution because it is likely much smaller than the Galactic disk contribution to τ_g that is itself small for the known FRBs. We then redraw the τ –DM relation in **Figure 16b**, which shows the broadening time versus DM using only the extragalactic components of both quantities.

In the figure, we also show the Galactic pulsar τ –DM relation under the assumption that extragalactic scattering comes from only the host galaxy. To compare extragalactic with Galactic scattering, we need to compensate for geometrical differences between the spherical waves from nearby sources and plane waves from/to distant sources/observers. The scattering time τ is thus a factor of three greater for scattering in the host galaxy than that implied by the Galactic τ –DM relation. The figure therefore shows the Galactic τ –DM band after shifting the Galactic scaling law of **Figure 16** upward by a factor of three.

8. SOURCES, RADIATION PROCESSES, AND CENTRAL ENGINES

The aggregate properties of FRBs, to the extent that they are now known, require explanations for the bursts themselves—duration, time-frequency structure, polarization, energetics, and, for repeating FRBs, their low duty cycle, absence of periodicity, and rate variability—as well as their population properties, including the sky rate versus fluence distribution, which are linked to their spatial distribution and beaming properties. All these contribute to a determination and physical understanding of the underlying sources.

8.1. Radiation Processes and Beaming

Emission processes for FRBs are probably most closely related to those for radio pulsars, for which there is a vast literature that is too large to be reviewed here. Similarities with coherent cyclotron radiation from planets and brown dwarfs may also be related at least by analogy.

Empirically, bursts necessarily comprise coherent, polarized shot pulses whose short durations (about nanoseconds) must be on the order of the reciprocal of the spectral width (approximately gigahertz) and combine incoherently in large numbers, with either a shot-rate variation or amplitude variation, to form the much longer burst durations (about milliseconds). Individual shots like those seen from the Crab pulsar (Hankins & Eilek 2007, Jessner et al. 2010) are prototypes for FRB shot pulses (Cordes & Wasserman 2016). A feature of modulated shot noise is that bursts with multipeaked structure are natural outcomes as are spectral modulations on the reciprocal timescale ($\sim 1 \mu\text{s}^{-1} - 1 \text{ ms}^{-1} = \text{kHz-MHz}$) (Cordes et al. 2004).

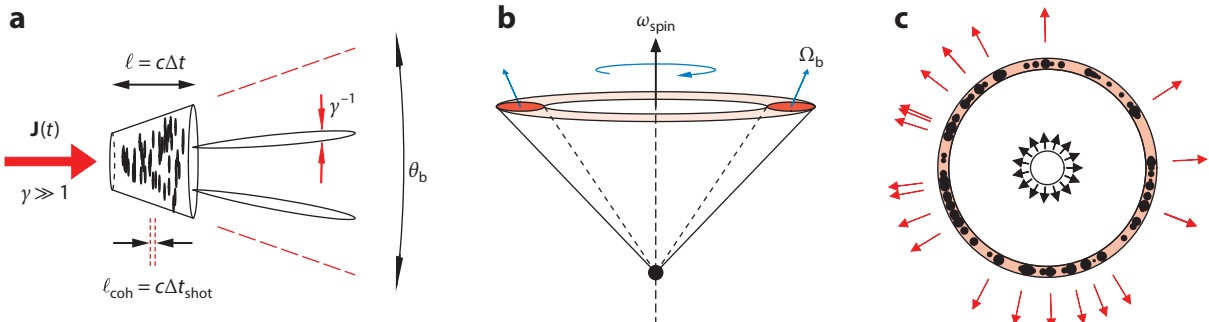


Figure 17

Possible beaming geometries for FRB sources. (a) A relativistic jet spanning an angle θ_b much larger than single particle beaming angles $\sim \gamma^{-1}$. Individual coherent emitters of size ℓ_{coh} are contained in an extended region of depth $\ell \sim cW$, where W is the FRB duration. The jet beam solid angle is $\sim \theta_b^2$. (b) A rotating beam comprising a relativistic jet swept around by rotation and covering a total solid angle $\Omega \sim 2\pi\sqrt{\Omega_b}$. (c) Quasi-isotropic mission from a spherical shell containing individual coherent emitters with a total solid angle $\Omega \sim 4\pi f_{coh}$, where f_{coh} is the fraction of the shell with active emitters. Abbreviation: DM, dispersion measure.

Relativistic beaming with large Lorentz factors γ is certainly involved with the emission process given the burst energetics discussed in Section 2.7, but it is not clear if beaming plays a role in burst durations and morphology. **Figure 17** shows three beaming configurations. First is a nonrotating jetted beam that might arise from magnetic reconnection (and would be two sided) or from a jet aligned with the spin axis of a compact object. Its orientation might change only slowly, so burst durations and substructure would be associated with temporal modulations of the particle flow or radiation coherence. The middle frame shows a rotating pulsar-like beam that sweeps through a more solid angle than that of the beam itself and might produce polarization changes like those seen from pulsars. Last is quasi-isotropic radiation involving local coherent beams associated with regions where coherent emission can be established, such as by particle beams injected into shocked gas. In this case the total solid angle is 4π multiplied by a subbeam filling factor. Other physical processes may also be described with these rotating versus nonrotating paradigms.

The emitted luminosity of an individual source is determined by the radiation physics, but the measured flux density (and luminosity \mathcal{L} defined earlier) depends on beam orientations. Individual pulsars, for comparison, show significant variability of pulse shapes and amplitudes, indicating stochasticity of the radiation process that should also be anticipated for FRBs and is seen in the repeater FRB 121102. The population luminosity function is a combination of these factors with the spatial distribution of sources. For pulsars, \mathcal{L} spans at least five decades due to the combination of radiation stochasticity, beaming geometry, and spatial distribution (e.g., Arzoumanian et al. 2002) along with scintillations, so \mathcal{L} will span an even greater range for the more widely distributed FRBs.

Radiation coherence makes N particles radiate with N^2 times the single-particle emission and is responsible for the high efficiency that is needed given the large energy in radio emission alone. The underlying particle acceleration may be linear (e.g., field-aligned electrostatic waves) or transverse (curvature and gyro-synchrotron radiation), but a coherence mechanism must also operate. An antenna mechanism involves particle bunches $\sim \lambda$ in size (modulo beaming) with many charged particles. Maser mechanisms require special distributions in momentum space to provide amplification. A maser (e.g., Luo & Melrose 1992) has the advantage of cumulative growth of radiation amplitudes over a region $\gg \lambda$, which may alleviate energy requirements that challenge coherent curvature radiation from bunches (Cordes & Wasserman 2016, Ghisellini & Locatelli 2018,

Lu & Kumar 2018). Nonetheless, emission is limited to the energy carried by particles, which are likely to be strongly dissipated by radiation reaction from radio emission alone.

Polarization may provide some clues. As mentioned in Section 2.5 for FRB 121102 and several other FRBs, the approximate constancy of the position angle across bursts contrasts with that often seen in pulsars, suggesting a nonrotating beam (as mentioned earlier) or a grazing beam in which a magnetic axis does not make a close approach with the line of sight (e.g., Backer et al. 1976, Beskin & Philippov 2012). The 100% linear polarization of bursts from FRB 121102 is similar to the polarization of some pulsars, but pulsars often show some circular polarization.

The spectral islands seen from several FRBs with \sim 0.1–0.5 GHz widths are distinct from Galactic scintillations and suggest a bandlimited emission process, such as one where the local plasma or cyclotron frequency (or their harmonics) is involved. The electron-cyclotron maser process is well established for planetary emission, including Earth’s auroral kilometric radiation (AKR) (Treumann 2006, Vorgul et al. 2011) and solar bursts (Chen et al. 2017), and produces 100% circular polarization, contrary to FRB emission. An e^\pm plasma would show no net circular polarization in the simplest case but allows linear polarization. Measured radiation might be, however, a combination of emission with normal EM modes that are linearly polarized in the magnetosphere followed by maser amplification without any polarization conversion. A cyclotron frequency $\nu_c \sim 1$ GHz corresponds to $B \sim 360\gamma$ G that is encountered at a radius $r \sim \gamma^{-1/3} 10^{10}$ cm for a magnetar with a surface field of 10^{15} G. This exceeds or is a good fraction of the light-cylinder radius for modest γ but would require a very large γ to be within the light cylinder of a millisecond magnetar. This context is similar to that for pulsars, which show polarization transfer effects and differential refraction (Barnard & Arons 1986, Wang et al. 2010), so similar complexity and diversity is to be expected from FRBs. A distinction from pulsars is the variability of the spectral islands, suggesting retuning of the emission process between bursts (if intrinsic) that might be accompanied by beam wandering (e.g., Katz 2017).

The absence of an observed periodicity in FRB 121102 may indicate a nonrotating object, but it is easy to destroy periodicities by chaotic precession from a star with a stochastic moment of inertia tensor (e.g., crustquakes) or from lensing that produces multiple bursts with rapidly changing delays. The epoch-dependent burst rate may have similar intrinsic or extrinsic causes. An additional extrinsic variability mechanism is triggering by injection of asteroids into a magnetosphere (Dai et al. 2016, Huang & Geng 2016). Asteroids are difficult to inject in rapid rotators ($\lesssim 0.5$ -s periods), however, because they are evaporated well before they reach the light cylinder (Cordes & Shannon 2008).

8.2. Source Models

The number of proposed source models has long exceeded the number of detected FRBs. Fortunately, the current rapid increase in burst numbers is not accompanied by a proportionate number of models. In fact, most (but certainly not all) attention is now paid to two paradigms, those involving isolated or binary compact objects [white dwarf (WD), NS, and BH] and AGNs, perhaps interacting with NSs. The much larger slate of models has included technomarkers from extragalactic civilizations (Lingam & Loeb 2017), superconducting cosmic strings (Yu et al. 2014; Thompson 2017a,b), exploding BHs (Barrau et al. 2014), reconnection in magnetars triggered by axion quark nuggets (van Waerbeke & Zhitnitsky 2019), WD–NS binaries (Gu et al. 2016), NS–NS mergers (Yamasaki et al. 2018), WD–BH mergers that create reconnecting magnetic blobs (Li et al. 2018a), collapse of supramassive NSs (Falcke & Rezzolla 2014), novae of exotic objects (quark or axion stars), accretion or interaction of asteroids with compact objects (e.g., WD, NS, BH; Mottez & Zarka 2014), mergers of compact objects, and births of NSs or BHs, as well as AGN–NS interactions and energetic activity (flares and starquakes) from magnetars.

Some of these produce GRBs from which associated prompt radio bursts have long been looked for. However, unless beaming radically increases the prompt radio burst rate, the GRB rate is too small by a factor of $\sim 10^3$ – 10^4 to account for FRBs. Models have been suggested for intermittent pulsars and RRATs (e.g., Luo & Melrose 2007) that might be relevant to FRBs but the vastly different energetics may make these models less relevant.

It is not our goal to review this rich diversity, especially given page and reference list limits. More details about the wide range of models may be found in other reviews (Katz 2016a, Popov et al. 2018). Instead, we build upon the fundamental quantities summarized in Section 2 on burst rates, repeatability, and energetics to suggest that compact objects and especially NSs are prime candidates for the underlying engines of many or most FRBs because they exist in sufficient numbers in the Universe (an NS born roughly every second in a Hubble volume) and possess sources of free energy (rotation, magnetic) that can account for burst energetics. Other objects may of course also generate radio bursts but perhaps at much lower rates.

Although energy reservoirs are available, channeling it into high brightness, coherent pulses with millisecond durations is more challenging, particularly because pulses are isolated, without obvious pre- or postursors, and they certainly do not occur as ongoing, high duty cycle processes. This contrasts with coherent solar bursts and radio flares, for example.

8.3. Demographics

Paradoxically, familiar objects in the Universe are too numerous to account for the very large all-sky FRB rate (10^3 – 10^4 d $^{-1}$), even if the beaming fraction is small. Special objects or special circumstances are needed. NSs are a good reference population because they can provide free energy from rotation, magnetic fields, and gravity. In the Universe there are $\sim 10^{17}$ – 10^{18} NSs in a Hubble volume (see the sidebar titled Neutron Star Populations in the Universe). Most pass through the pulsar channel involving birth spin rates ~ 10 – 100 ms, electromagnetic radiation across the entire spectrum including prominent coherent radio emission, spindown, and termination of e^\pm pair production and, thus, also the radio emission after 10–100 Myr. If all NSs in a Hubble volume are linked to FRBs, only about one event per NS is needed to account for the sky rate. Clearly, only a tiny subset of NSs can be involved given the >200 events seen from FRB 121102.

FRB directions appear to be isotropic. That the first FRB localization was to a dwarf, star-forming galaxy rather than a massive L * -type galaxy suggests that FRBs do not follow star formation generally but reside in host galaxies that are themselves special. This sample-of-one situation

NEUTRON STAR POPULATIONS IN THE UNIVERSE

Extragalactic NSs formed over cosmological time are potential sources of superstrong bursts whose number per NS, $N_b = \eta_b T_b$, may be large or small (where η_b = burst rate per NS during a burst phase of duration T_b). The aggregate burst rate follows the NS birth rate, Γ_{ns} . Scaling from the Galactic NS formation rate per unit stellar mass, $\dot{n}_{\text{ns,M}} \approx \dot{n}_{\text{ns,M},-13} 10^{-13}$ year $^{-1}$ M $^{-1}_\odot$ (e.g., one NS every 100 years per 10^{11} M $_\odot$ in stars), and the stellar mass density $\rho_\star = \Omega_\star \rho_c$, where $\rho_c = 3H_0^2/8\pi G$ is the closure density and $\Omega_\star \approx 0.003\Omega_{*,0.003}$ (Read & Trentham 2005), about $N_{\text{ns}} \sim 10^{17}$ NSs are produced in a Hubble volume $V_H = 4\pi d_H^3/3$ for a Hubble distance $d_H = c/H_0 = 4.3h_{0.7}^{-1}$ Gpc and a typical galaxy age $T_{\text{gal}} = 10$ Gyr. A higher star formation rate at redshifts ~ 0.5 – 2 increases the number by about a factor of ten (Nicholl et al. 2017, and references therein). The aggregate NS birth is then $\Gamma_{\text{ns}} = \rho_\star \Omega_\star \dot{n}_{\text{ns,M}} V_H \sim 4 \times (10^4\text{--}10^5)$ day $^{-1}$ h $_{0.7}^{-1}$ $\dot{n}_{\text{ns,M},-13} \Omega_{*,0.003}$ and the corresponding burst rate is $\Gamma_b = N_b \Gamma_{\text{ns}}$. For burst detections out to a distance $d_{\text{max}} \ll d_H$ (modulo a proper cosmological integration), $\Gamma_b \approx N_b \Gamma_{\text{ns}} (d_{\text{max}}/d_H)^3$, illustrating the tradeoff between N_b and d_{max} in matching to the empirical FRB rate, Γ_{frb} .

may change with subsequent localizations, but the simplest provisional conclusion is that FRBs are from special galaxies that produce appropriate central engines.

The magnetar channel accounts for \sim 10% of NSs (e.g., Popov et al. 2010). About 1% of NSs remain in binaries and become millisecond pulsars through accretion-driven spinup with radio lifetimes greater than about a gigayear. Another \sim 1% are in NS–NS binaries that ultimately merge, producing short-hard GRBs and chirped gravitational waves in the kilohertz band, like GW 170817 (Abbott et al. 2017).

If FRBs are largely one-off events per source, rendering repeaters such as FRB 121102 an outlier, FRBs could be associated with NS birth events or a highly unusual crustquake, accretion event, or magnetospheric discharge that occurs only once per NS and perhaps not to every NS. The aggregate event rate is then tied to the NS birth rate Γ_{ns} , which is within a factor of 10 of the empirical FRB rate, Γ_{frb} . For this to be the case, FRB events would be associated with a sizable fraction of all NSs, perhaps only the magnetar channel or some kind of rare event that happens to nearly all NSs. This scenario seems implausible because spin and magnetic energies of the different NSs differ by many orders of magnitude, implying that FRBs would be insensitive to this range, whereas the radio emission itself is extreme. Furthermore, it seems premature to dismiss the repeating FRB as an outlier because, as discussed earlier, spectrotemporal structure of some nonrepeating FRBs is similar to that of FRB 121102. One might dismiss this similarity as a feature of the radiation process rather than of the underlying engine, but there is currently no support for that view. Consequently, NS models can plausibly imply that most or all FRBs repeat, albeit at potentially different rates that have obscured the observational situation about repetitions.

8.4. Young, Rapidly Rotating Neutron Stars

Young, high-field NSs have been a particular focus of models since the early days of FRBs, and a self-consistent picture is emerging in favor of these models for at least the repeating FRB 121102 and its associated PRS. Broad features include a high magnetic field ($>10^{13}$ G), rapid rotation (spin period $P \sim$ ms), and a young age (\sim 10–100 years). The object must be old enough so that radio pulses are not free-free absorbed and young enough so that it can provide the luminosity of the PRS. Unresolved issues include whether the objects are magnetically powered or rotation powered and whether the coherent bursts themselves originate from the magnetosphere of the spinning object (i.e., within the light cylinder radius $r_{\text{lc}} = cP/2\pi$) as GPs in a pulsar-like model or from synchrotron maser activity in a distributed region well outside r_{lc} . Other differences between models concern the mass in the SN and pre-SN ejecta.

8.4.1. Giant pulse models. Analogs to GPs from the Crab pulsar (Connor et al. 2016b, Cordes & Wasserman 2016, Lyutikov et al. 2016, Popov & Pshirkov 2016) scale with burst amplitudes from the wide GP fluence distribution and from the spindown rate of the Crab pulsar. Coherent curvature radiation may underlie Crab GPs, but whether it can provide $\gtrsim 10^6$ larger fluences for FRBs is challenging though may be helped by local maser amplification or extrinsic lensing. One avenue of exploration is a monitoring program to probe the extent of the long tail of Crab GPs. Constraints on GPs from NSs likely apply to other central engines, including exotic sources, because the issues in generating powerful fast bursts are generic.

8.4.2. Magnetar models and superluminous supernovae. Magnetar (and similar) models for FRBs were suggested prior to the discovery of repeat bursts from FRB 121102 and its association with a PRS in a star-forming galaxy (e.g., Popov & Postnov 2010, Thornton et al. 2013, Lyubarsky 2014, Kulkarni et al. 2015, Pen & Connor 2015, Cordes & Wasserman 2016, Katz 2016b, Murase

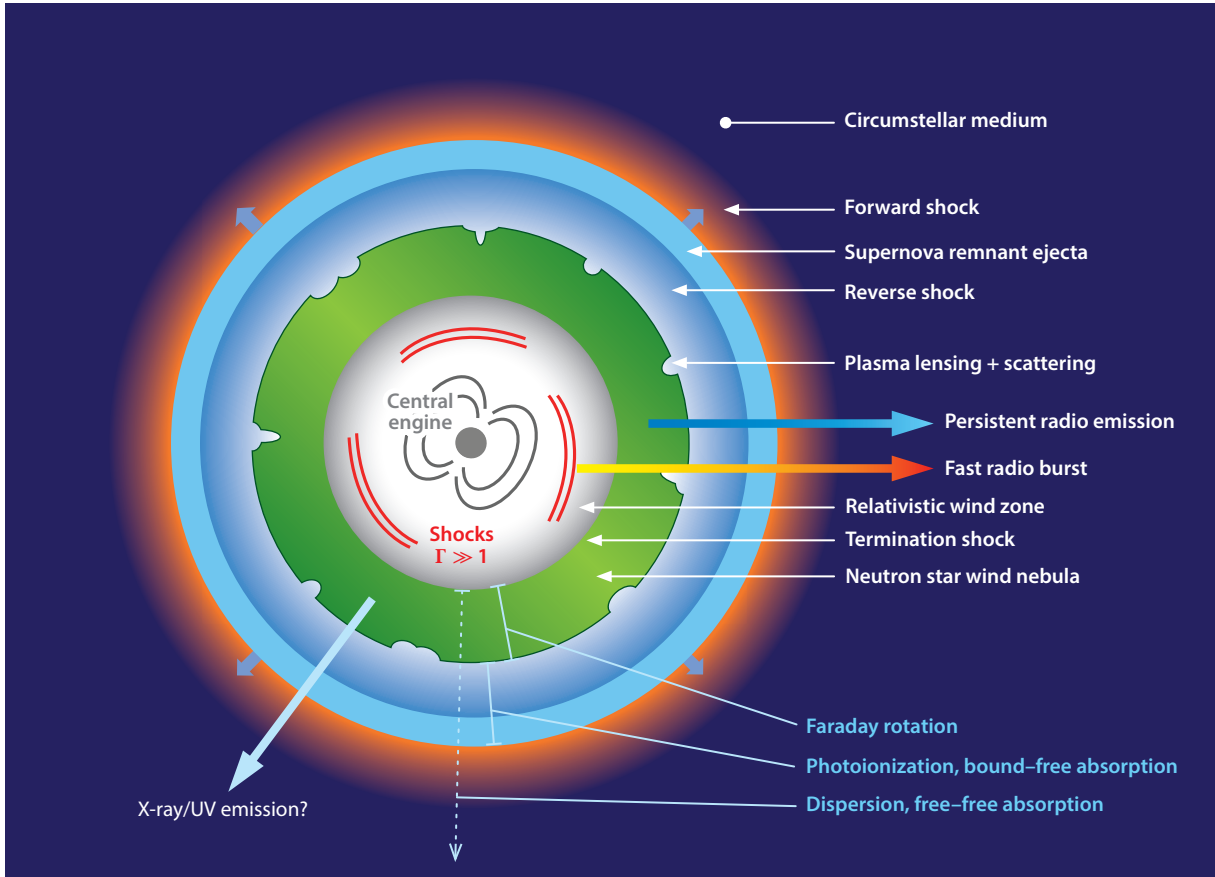


Figure 18

Schematic diagram of an FRB source engine involving a young, highly magnetized neutron star. Alternative models, such as compact objects orbiting AGNs, may share some (but not all) of the same features. Figure adapted from Margalit & Metzger (2018) and B. Metzger, private communication.

et al. 2016, Piro 2016). Subsequent work has identified a consistent picture for FRB 121102 in which the bursts and persistent source originate from the same structure, although details differ between different models (Kashiyama & Murase 2017, Waxman 2017, Margalit & Metzger 2018, Margalit et al. 2018). **Figure 18** illustrates the features of the Margalit & Metzger (2018) model. It is by no means clear that a magnetar model underlies all FRBs, but the case for the repeating FRB is strong because the model can account for many features of the bursts and the PRS. Even in the magnetar paradigm a great deal of diversity of FRB sources is expected from a range of ages, environments, and initial conditions of the sources.

Waxman (2017) used the radio light curve, angular broadening from VLBI, and radio spectrum to show consistency of the persistent source with a compact ($\sim 0.1\text{--}1$ pc) region emitting nonself-absorbed synchrotron radiation from gas heated by semirelativistic shells plowing into ambient gas. Other, highly relativistic shells produce FRBs from synchrotron maser emission at gigahertz frequencies determined by the local plasma and cyclotron frequencies. Negative absorption from this process is confined to roughly a 40% band. The age of the source is less than a few hundred years, and the dense outer shell that confines the persistent emission provides only a small DM

while providing an RM similar to the measured values. Waxman's analysis reached conclusions similar to those by Lyubarsky (2014), although the former paper assumes an e-p plasma and the latter a pair plasma produced in magnetar flares. Beloborodov (2017) made a similar analysis but invoked specific properties of magnetars to develop a flare-driven model, also with FRBs produced by synchrotron maser emission and a similar persistent source size.

The association of FRBs and persistent source(s) with SLSNe and long GRBs (Metzger et al. 2017) ties together the physics of central engines and circumsource media with the demographics of SLSNe in dwarf, star-forming galaxies. Though much of this hinges on FRB 121102, another source similar to its PRS has been identified (Law et al. 2018), and finding such sources may be a productive avenue for finding burst sources and testing the model and even for finding bursts. Omand et al. (2018) propose that high-frequency observations with the Atacama Large Millimeter/Submillimeter Array (ALMA) and the VLA can detect persistent sources at earlier, optically thin epochs than \sim 1–10 GHz. A recent ALMA observation of FRB 121102 placed an upper limit on any persistent continuum emission that was consistent with extrapolation of the low-frequency spectrum.

Other tests for general consistency with a central engine/outburst model include the epoch dependences of DM and RM along with the flux density of the PRS. If burst rates at present are enhanced by plasma lensing, then it too should vary. X-rays may discriminate between models in which FRBs dominate the EM budget (e.g., Waxman 2017) compared to those in which high-energy emission dominates, though absorption may prevent this for young objects (Margalit et al. 2018).

8.5. AGNs Interacting with Neutron Stars

Both AGNs and NSs are abundant in the Universe, and NS populations bound to AGNs are likely common. But rare interacting NS–AGN configurations may provide an appropriately sized population that yields low duty cycle bursts. Zhang (2017, 2018) presents a specific picture in which AGN outbursts trigger bursts from an NS; this is also suggested by Cordes & Wasserman (2016). A galaxy center is an alternative environment for providing a large RM, as demonstrated by the (old) GC magnetar J1745-2900 (Desvignes et al. 2018) with $\text{RM} \sim 10^5 \text{ rad m}^{-2}$ that is time variable. The model implies that bursts should show periodicity at the NS orbital period and associates burst polarization with the magnetic field that interacts with the AGN's jet flow. If a young magnetar is required to provide bright FRBs, it is not clear whether an external trigger or external magnetic field is really needed.

9. FRBs AS TOOLS FOR ASTROPHYSICS AND FUNDAMENTAL PHYSICS

Radio bursts are obvious probes of magnetized plasma of all kinds, and those originating at extragalactic distances give unique opportunities for remote sensing of the extreme environments around burst sources, their host galaxies, and the IGM, as discussed at length already. Continued monitoring of repeaters provides the means for testing models for central engines via epoch dependences of DM, RM, etc. Numerous papers have outlined the program for using FRBs to quantify the ionized IGM (as already summarized) and its large-scale structure (e.g., Masui & Sigurdson 2015). In the latter case, DMs of $\sim 10^4$ FRBs may yield a significant clustering signal under the assumption that local (host-galaxy and circumsource) DM contributions are small (Zhou et al. 2014). Currently, only the repeating FRB has relatively good constraints on local DM (and RM) contributions, but that will change as the FRB sample continues to grow rapidly. Probing cosmological magnetic fields using large FRB samples has been outlined by Vazza et al. (2018).

A large sample of FRBs is needed to fully ascertain the range of local DMs and contributions from galaxy clusters. Electron density models for the Milky Way are uncertain even with thousands of DM (and other) measurements because the number of lines of sight is too small to sample all prominent HII regions. Local DMs of FRBs may span a similar large range among the many host galaxies involved in a large FRB sample (Yang et al. 2017). Indeed, young-NS models imply that DM, RM, and free-free absorption will be large in the early days of a source and that FRB detections will occur only after they have declined sufficiently (e.g., Connor et al. 2016b, Pen & Connor 2015, Margalit & Metzger 2018). High- z FRBs benefit from having their local DMs reduced by a $(1+z)^{-1}$ factor, so the cosmology program may rely on identifying any large redshifts directly, which may be a challenge if only dwarf galaxies harbor FRB sources. Large-scale magnetic fields in the IGM (Zheng et al. 2014, Vazza et al. 2018) will benefit from large FRB numbers and will complement RM measurements from AGNs already available (Kronberg et al. 2008).

As previously mentioned, FRB constraints on microlensing and dark matter objects will improve greatly with both large numbers and detailed analyses of burst spectra that may be influenced by interference effects. Finally, FRBs place limits on the photon mass (Bonetti et al. 2016, Wu et al. 2016, Shao & Zhang 2017) but require independent redshifts and determinations of DM_{IGM} because a nonzero photon mass contributes an arrival time delay degenerate with that of plasma dispersion.

10. PROSPECTS FOR FUTURE WORK

The investigation of FRBs as a novel phenomenon has followed an explosive growth trajectory in its early phase, as measured by detections, theoretical models, publications, and citations. In the near term, increasing numbers of detections are assured. ASKAP in its fly’s-eye mode has shown remarkable success with large fields of view at low sensitivity (Bannister et al. 2017, Shannon et al. 2018), and CHIME, which views the whole sky daily as it passes overhead, has detected FRBs in its initial operations (CHIME/FRB Collab. et al. 2019a,b). However, neither telescope is likely to produce sufficiently precise localizations in the absence of new modes of operation or outrigger telescopes. The UTMOST has detected several FRBs (e.g., Caleb et al. 2017, Farah et al. 2018) but with limited localization precision in one dimension, joining blind surveys at single-dish telescopes with improved instrumentation (e.g., the ALPACA phased array feed at Arecibo) to increase the FRB sample.

Reliable measurements of FRB distances and energetics require host-galaxy identifications through better than arcsecond localizations. The *realfast* project (real-time fast transients at the VLA; Law et al. 2015) should yield more such blind localizations, as should surveys with the upgraded Apertif at the Westerbork Synthesis Radio Telescope (e.g., Oostrum et al. 2017), as well as MeerKAT. New telescope projects like the 110-dish Deep Synoptic Array (DSA-110) and the Hydrogen Intensity and Real-time Analysis eXperiment (HIRAX) also promise a future yield of blind detections with precise localizations. A complementary approach is the targeted follow-up of blind FRB detections at higher sensitivity (e.g., with the Arecibo or FAST telescopes) in order to identify other repeating sources that can then be subjected to intensive interferometric campaigns, as is done for FRB 121102 (Chatterjee et al. 2017, Marcote et al. 2017).

The detection of rare weak bursts in massive volumes of survey data is a difficult problem, made more challenging by the steadily worsening RFI environment. Machine learning techniques have been proposed (Connor & van Leeuwen 2018) and have already demonstrated dramatic results (Zhang et al. 2018), and cross-disciplinary collaboration will continue to bear fruit. Manifestation of the cosmologically nearby FRB population is probably limited by the low burst rate per source, but sufficient dwell times on galaxy clusters (e.g., Fialkov et al. 2018) may provide detections of

nearby galaxies that are easier to characterize than more distant ones. If our Galaxy (or a neighboring one) hosts an FRB source, we might experience rare but extraordinarily bright bursts with (relatively) low pulse DM. Such bursts would be difficult to distinguish from RFI but may be detectable with all-sky dipole antennas or as a citizen science project using mobile phone receivers (e.g., Katz 2014a, Maoz & Loeb 2017).

Eventually, efficient petascale computation may allow next-generation projects like the DSA-2000 (a proposed 2000-dish successor to DSA-110) and the full Square Kilometre Array (SKA) (e.g., Macquart et al. 2015) to continuously image large swathes of the sky at high-enough time resolution to routinely detect and localize large samples of FRBs. Rather like the Large Synoptic Survey Telescope (LSST) event streams, the primary challenge will be the efficient allocation of follow-up resources to extract scientific value from those detections—no doubt a much better problem to have than the current situation.

DISCLOSURE STATEMENT

The authors are not aware of any affiliations, memberships, funding, or financial holdings that might be perceived as affecting the objectivity of this review.

ACKNOWLEDGMENTS

We thank our colleagues and collaborators for discussions and help, as well as access to some results in advance of publication. An incomplete list includes Matthew Bailes, Keith Bannister, Cees Bassa, Nick Battaglia, Edo Berger, Geoff Bower, Patrick Boyle, Sarah Burke-Spolaor, Manisha Caleb, Fernando Camilo, Liam Connor, Adam Deller, Klaus Dolag, Jean Eilek, Ron Ekers, Wael Farah, Griffin Foster, Dale Frail, Bryan Gaensler, Vishal Gajjar, Avishay Gal-Yam, Tim Hankins, Gregg Hallinan, Jason Hessels, Assaf Horesh, Simon Johnston, David Kaplan, Vicky Kaspi, Jonathan Katz, Evan Keane, Michael Kramer, Shri Kulkarni, Casey Law, Avi Loeb, Duncan Lorimer, Ryan Lynch, J.P. Macquart, Elizabeth Mahoney, Benito Marcote, Maura McLaughlin, Daniele Michilli, Chiara Mingarelli, Ben Margalit, Brian Metzger, Eran Ofek, Stefan Oslowski, Zsolt Paragi, Emily Petroff, Vikram Ravi, Paul Scholz, Andrew Seymour, Ryan Shannon, Andrew Siemion, Lorenzo Sironi, Laura Spitler, Shriharsh Tendulkar, Shen Wang, Eli Waxman, Ira Wasserman, Robert Wharton, Barak Zackay, Bing Zhang, Yunfan (Gerry) Zhang, and Weiwei Zhu. The authors acknowledge support from the National Science Foundation (AAG 1815242), and are members of the NANOGrav Physics Frontiers Center, which is supported by the National Science Foundation award number 1430284.

LITERATURE CITED

- Abbott BP, Abbott R, Abbott TD, et al. 2017. *Ap. J. Lett.* 848:L13
Amy SW, Large MI, Vaughan AE. 1989. *Publ. Astron. Soc. Aust.* 8:172–75
Arzoumanian Z, Chernoff DF, Cordes JM. 2002. *Ap. J.* 568:289–301
Backer DC, Rankin JM, Campbell DB. 1976. *Nature* 263:202–7
Baird GA, Delaney TJ, Lawless BG, et al. 1975. *Ap. J. Lett.* 196:L11–13
Bannister KW, Shannon RM, Macquart JP, et al. 2017. *Ap. J. Lett.* 841:L12
Bannister KW, Stevens J, Tuntsov AV, et al. 2016. *Science* 351:354–56
Barnard JJ, Arons J. 1986. *Ap. J.* 302:138
Barrau A, Rovelli C, Vidotto F. 2014. *Phys. Rev. D* 90:127503
Bassa CG, Tendulkar SP, Adams EAK, et al. 2017. *Ap. J. Lett.* 843:L8

- Beloborodov AM. 2017. *Ap. J. Lett.* 843:L26
- Beskin VS, Philippov AA. 2012. *MNRAS* 425:814–40
- Bhandari S, Keane EF, Barr ED, et al. 2018. *MNRAS* 475:1427–46
- Bonetti L, Ellis J, Mavromatos NE, et al. 2016. *Phys. Lett. B* 757:548–52
- Bower GC, Rao R, Krips M, et al. 2018. *Astron. J.* 155:227
- Bower GC, Wright MCH, Falcke H, Backer DC. 2003. *Ap. J.* 588:331–37
- Caleb M, Flynn C, Bailes M, et al. 2016. *MNRAS* 458:718–25
- Caleb M, Flynn C, Bailes M, et al. 2017. *MNRAS* 468:3746–56
- Caleb M, Keane EF, van Straten W, et al. 2018. *MNRAS* 478:2046–55
- Champion DJ, Petroff E, Kramer M, et al. 2016. *MNRAS* 460:L30–34
- Chatterjee S, Law CJ, Wharton RS, et al. 2017. *Nature* 541:58–61
- Chawla P, Kaspi VM, Josephy A, et al. 2017. *Ap. J.* 844:140
- Chen L, Wu DJ, Zhao GQ, Tang JF. 2017. *J. Geophys. Res. (Space Phys.)* 122:35–49
- CHIME/FRB Collab., Amiri M, Bandura K, et al. 2018. *Ap. J.* 863:48
- CHIME/FRB Collab., Amiri M, Bandura K, et al. 2019a. *Nature* 566:230–34
- CHIME/FRB Collab., Amiri M, Bandura K, et al. 2019b. *Nature* 566:235–38
- Connor L, Pen UL, Oppermann N. 2016a. *MNRAS* 458:L89–93
- Connor L, Sievers J, Pen UL. 2016b. *MNRAS* 458:L19–23
- Connor L, van Leeuwen J. 2018. *Astron. J.* 156:256
- Cordes JM, Bhat NDR, Hankins TH, et al. 2004. *Ap. J.* 612:375–88
- Cordes JM, Lazio TJW. 2002. arXiv:astro-ph/0207156
- Cordes JM, McLaughlin MA. 2003. *Ap. J.* 596:1142–54
- Cordes JM, Rickett BJ. 1998. *Ap. J.* 507:846–60
- Cordes JM, Shannon RM. 2008. *Ap. J.* 682:1152–65
- Cordes JM, Wasserman I. 2016. *MNRAS* 457:232–57
- Cordes JM, Wasserman I, Hessels JWT, et al. 2017. *Ap. J.* 842:35
- Cordes JM, Wharton RS, Spitler LG, et al. 2016. arXiv:1605.05890
- Dai ZG, Wang JS, Wu XF, Huang YF. 2016. *Ap. J.* 829:27
- Dennison B. 2014. *MNRAS* 443:L11–14
- Dessenne CAC, Green DA, Warner PJ, et al. 1996. *MNRAS* 281:977–84
- Desvignes G, Eatough RP, Pen UL, et al. 2018. *Ap. J. Lett.* 852:L12
- Dolag K, Gaensler BM, Beck AM, Beck MC. 2015. *MNRAS* 451:4277–89
- Draine BT. 2011. *Physics of the Interstellar and Intergalactic Medium*. Princeton, NJ: Princeton Univ. Press
- Edwards PJ, Hurst RB, McQueen MPC. 1974. *Nature* 247:444–46
- Eftekhari T, Berger E. 2017. *Ap. J.* 849:162
- Eftekhari T, Berger E, Williams PKG, Blanchard PK. 2018. *Ap. J.* 860:73
- Eichler D. 2017. *Ap. J.* 850:159
- Falcke H, Rezzolla L. 2014. *Astron. Astrophys.* 562:A137
- Farah W, Bailes M, Jameson A, et al. 2017. *Astron. Telegr.* #10867
- Farah W, Bailes M, Jameson A, et al. 2018. *Astron. Telegr.* #11675
- Fialkov A, Loeb A, Lorimer DR. 2018. *Ap. J.* 863:132
- Fiedler RL, Dennison B, Johnston KJ, Hewish A. 1987. *Nature* 326:675–78
- Fruchter AS, Levan AJ, Strolger L, et al. 2006. *Nature* 441:463–68
- Gajjar V, Siemion APV, Price DC, et al. 2018. *Ap. J.* 863:2
- Ghisellini G, Locatelli N. 2018. *Astron. Astrophys.* 613:A61
- Graham Smith F, Lyne AG, Jordan C. 2011. *MNRAS* 410:499–503
- Gu WM, Dong YZ, Liu T, et al. 2016. *Ap. J. Lett.* 823:L28
- Hankins TH, Eilek JA. 2007. *Ap. J.* 670:693–701
- Hankins TH, Rickett BJ. 1975. In *Methods in Computational Physics: Advances in Research and Applications, Volume 14—Radio Astronomy*, ed. B Alder, S Fernbach, M Rotenberg, pp. 55–129. New York: Academic
- Hessels JWT, Spitler LG, Seymour AD, et al. 2019. *Ap. J. Lett.* 876:L23

- Huang YF, Geng JJ. 2016. In *Frontiers in Radio Astronomy and FAST Early Sciences Symposium 2015*, ed. L Qain. *ASP Conf. Ser.* 502:1. San Francisco: ASP
- Hughes VA, Retallack DS. 1973. *Nature* 242:105–7
- Huguenin GR, Moore EL. 1974. *Ap. J. Lett.* 187:L57
- Hyman SD, Lazio TJW, Kassim NE, et al. 2005. *Nature* 434:50–52
- Inoue S. 2004. *MNRAS* 348:999–1008
- Ioka K. 2003. *Ap. J. Lett.* 598:L79–82
- Jackson JD. 1962. *Classical Electrodynamics*. New York: Wiley
- Jessner A, Popov MV, Kondratiev VI, et al. 2010. *Astron. Astrophys.* 524:A60
- Karastergiou A, Chennamangalam J, Armour W, et al. 2015. *MNRAS* 452:1254–62
- Kashiyama K, Murase K. 2017. *Ap. J. Lett.* 839:L3
- Katz JI. 2014a. *Phys. Rev. D* 89:103009
- Katz JI. 2014b. arXiv:1409.5766
- Katz JI. 2016a. *Mod. Phys. Lett. A* 31:1630013
- Katz JI. 2016b. *Ap. J.* 826:226
- Katz JI. 2017. *MNRAS* 467:L96–99
- Keane EF, Barr ED, Jameson A, et al. 2018. *MNRAS* 473:116–35
- Keane EF, Johnston S, Bhandari S, et al. 2016. *Nature* 530:453–56
- Keane EF, Petroff E. 2015. *MNRAS* 447:2852–56
- Kronberg PP, Bernet ML, Miniati F, et al. 2008. *Ap. J.* 676:70–79
- Kulkarni SR, Ofek EO, Neill JD. 2015. arXiv:1511.09137
- Kulkarni SR, Ofek EO, Neill JD, et al. 2014. *Ap. J.* 797:70
- Lambert HC, Rickett BJ. 1999. *Ap. J.* 517:299–317
- Law CJ, Abruzzo MW, Bassa CG, et al. 2017. *Ap. J.* 850:76
- Law CJ, Bower GC, Burke-Spolaor S, et al. 2015. *Ap. J.* 807:16
- Law CJ, Gaensler BM, Metzger BD, et al. 2018. *Ap. J. Lett.* 866:L22
- Lawrence E, Vander Wiel S, Law C, et al. 2017. *Astron. J.* 154:117
- Li LB, Huang YF, Geng JJ, Li B. 2018a. *Res. Astron. Astrophys.* 18:061
- Li ZX, Gao H, Ding XH, et al. 2018b. *Nat. Commun.* 9:3833
- Lingam M, Loeb A. 2017. *Ap. J. Lett.* 837:L23
- Linscott IR, Erkes JW. 1980. *Ap. J. Lett.* 236:L109–13
- Loeb A, Shvartzvald Y, Maoz D. 2014. *MNRAS* 439:L46–50
- Lorimer DR, Bailes M, McLaughlin MA, et al. 2007. *Science* 318:777–80
- Lu W, Kumar P. 2018. *MNRAS* 477:2470–93
- Luan J, Goldreich P. 2014. *Ap. J. Lett.* 785:L26
- Luo Q, Melrose D. 2007. *MNRAS* 378:1481–90
- Luo Q, Melrose DB. 1992. *MNRAS* 258:616–20
- Luo R, Lee K, Lorimer DR, Zhang B. 2018. *MNRAS* 481:2320–37
- Lyubarsky Y. 2014. *MNRAS* 442:L9–13
- Lyutikov M, Burzawa L, Popov SB. 2016. *MNRAS* 462:941–50
- Macquart JP, Ekers R. 2018a. *MNRAS* 480:4211–30
- Macquart JP, Ekers RD. 2018b. *MNRAS* 474:1900–8
- Macquart JP, Johnston S. 2015. *MNRAS* 451:3278–86
- Macquart JP, Keane E, Grainge K, et al. 2015. In *Proceedings of Advancing Astrophysics with the Square Kilometre Array (AASKA14), Giardini Naxos, Italy, June 9–13, 2014*, id.055. Proceedings of Science. <https://pos.sissa.it/215/055/pdf>
- Macquart JP, Koay JY. 2013. *Ap. J.* 776:125
- MAGIC Collab., Acciari VA, Ansoldi S, et al. 2018. *MNRAS* 481:2479–86
- Mahony EK, Ekers RD, Macquart JP, et al. 2018. *Ap. J.* 867:L10
- Main R, Yang IS, Chan V, et al. 2018. *Nature* 557:522–25
- Manchester RN, Hobbs GB, Teoh A, Hobbs M. 2005. *Astron. J.* 129:1993–2006
- Maoz D, Loeb A. 2017. *MNRAS* 467:3920–23

- Maoz D, Loeb A, Shvartzvald Y, et al. 2015. *MNRAS* 454:2183–89
- Marcote B, Paragi Z, Hessels JWT, et al. 2017. *Ap. J. Lett.* 834:L8
- Margalit B, Metzger BD. 2018. *Ap. J. Lett.* 868:L4
- Margalit B, Metzger BD, Berger E, et al. 2018. *MNRAS* 481:2407–26
- Marrone DP, Moran JM, Zhao JH, Rao R. 2007. *Ap. J. Lett.* 654:L57–60
- Masui K, Lin HH, Sievers J, et al. 2015. *Nature* 528:523–25
- Masui KW, Sigurdson K. 2015. *Phys. Rev. Lett.* 115:121301
- McLaughlin MA, Lyne AG, Lorimer DR, et al. 2006. *Nature* 439:817–20
- McQuinn M. 2014. *Ap. J. Lett.* 780:L33
- Metzger BD, Berger E, Margalit B. 2017. *Ap. J.* 841:14
- Michilli D, Seymour A, Hessels JWT, et al. 2018. *Nature* 553:182–85
- Mottez F, Zarka P. 2014. *Astron. Astrophys.* 569:A86
- Muñoz JB, Kovetz ED, Dai L, Kamionkowski M. 2016. *Phys. Rev. Lett.* 117:091301
- Murase K, Kashiyama K, Mészáros P. 2016. *MNRAS* 461:1498–511
- Narayan R. 1992. *Philos. Trans. R. Soc. A* 341:151–65
- Nicastro F, Kaastra J, Krongold Y, et al. 2018. *Nature* 558:406–9
- Nicholl M, Williams PKG, Berger E, et al. 2017. *Ap. J.* 843:84
- Ofek EO. 2017. *Ap. J.* 846:44
- Olausen SA, Kaspi VM. 2014. *Ap. J. Suppl.* 212:6
- Omand CMB, Kashiyama K, Murase K. 2018. *MNRAS* 474:573–79
- Oostrum LC, van Leeuwen J, Attema J, et al. 2017. *Astron. Telegr.* #10693
- Oppermann N, Connor LD, Pen UL. 2016. *MNRAS* 461:984–87
- O’Sullivan JD, Ekers RD, Shaver PA. 1978. *Nature* 276:590
- Palaniswamy D, Li Y, Zhang B. 2018. *Ap. J. Lett.* 854:L12
- Palaniswamy D, Wayth RB, Trott CM, et al. 2014. *Ap. J.* 790:63
- Palmer DM. 1993. *Ap. J. Lett.* 417:L25–28
- Patel C, Agarwal D, Bhardwaj M, et al. 2018. *Ap. J.* 869:181
- Pen UL, Connor L. 2015. *Ap. J.* 807:179
- Perley DA, Levan AJ, Tanvir NR, et al. 2013. *Ap. J.* 778:128
- Petroff E, Bailes M, Barr ED, et al. 2015a. *MNRAS* 447:246–55
- Petroff E, Barr ED, Jameson A, et al. 2016. *Publ. Astron. Soc. Aust.* 33:e045
- Petroff E, Burke-Spolaor S, Keane EF, et al. 2017a. *MNRAS* 469:4465–82
- Petroff E, Houben L, Bannister K, et al. 2017b. arXiv:1710.08155
- Petroff E, Johnston S, Keane EF, et al. 2015b. *MNRAS* 454:457–62
- Petroff E, Keane EF, Barr ED, et al. 2015c. *MNRAS* 451:3933–40
- Petroff E, van Straten W, Johnston S, et al. 2014. *Ap. J. Lett.* 789:L26
- Piro AL. 2016. *Ap. J. Lett.* 824:L32
- Popov SB, Pons JA, Miralles JA, et al. 2010. *MNRAS* 401:2675–86
- Popov SB, Postnov KA. 2010. In *Evolution of Cosmic Objects through their Physical Activity*, ed. HA Harutyunian, AM Mickaelian, Y Terzian, pp. 129–33. Yerevan: Natl. Acad. Sci. Repub. Armen.
- Popov SB, Postnov KA, Pshirkov MS. 2018. *Phys.-Uspekhi* 61(10):1063–79
- Popov SB, Pshirkov MS. 2016. *MNRAS* 462:L16–20
- Price DC, Gajjar V, Dhar A, et al. 2018. *Astron. Telegr.* #11376
- Prochaska JX, Neeleman M. 2018. *MNRAS* 474:318–25
- Ramachandran R, Mitra D, Deshpande AA, et al. 1997. *MNRAS* 290:260–64
- Ravi V, Shannon RM, Bailes M, et al. 2016. *Science* 354:1249–52
- Read JI, Trentham N. 2005. *Philos. Trans. R. Soc. Lond. Ser. A* 363:2693–710
- Rees MJ. 1977. *Nature* 266:333–34
- Reines AE, Sivakoff GR, Johnson KE, Brogan CL. 2011. *Nature* 470:66–68
- Rickett BJ. 1990. *Annu. Rev. Astron. Astrophys.* 28:561–605
- Scholz P, Bogdanov S, Hessels JWT, et al. 2017. *Ap. J.* 846:80
- Scholz P, Spitler LG, Hessels JWT, et al. 2016. *Ap. J.* 833:177

- Seth AC, van den Bosch R, Mieske S, et al. 2014. *Nature* 513:398–400
- Shannon RM, Macquart JP, Bannister KW, et al. 2018. *Nature* 562:386–90
- Shao L, Zhang B. 2017. *Phys. Rev. D* 95:123010
- Shull JM, Danforth CW. 2018. *Ap. J. Lett.* 852:L11
- Siemion APV, Bower GC, Foster G, et al. 2012. *Ap. J.* 744:109
- Spitler LG, Cordes JM, Hessels JWT, et al. 2014. *Ap. J.* 790:101
- Spitler LG, Herrmann W, Bower GC, et al. 2018. *Ap. J.* 863:150
- Spitler LG, Scholz P, Hessels JWT, et al. 2016. *Nature* 531:202–5
- Suresh A, Cordes JM. 2019. *Ap. J.* 870:29
- Tanenbaum BS, Zeissig GA, Drake FD. 1968. *Science* 160:760
- Taylor JH, Huguenin GR, Hirsch RM. 1972. *Ap. J. Lett.* 172:L17
- Tendulkar SP, Bassa CG, Cordes JM, et al. 2017. *Ap. J. Lett.* 834:L7
- Thompson C. 2017a. *Ap. J.* 844:65
- Thompson C. 2017b. *Ap. J.* 844:162
- Thornton D, Stappers B, Bailes M, et al. 2013. *Science* 341:53–56
- Tominaga N, Niino Y, Totani T, et al. 2018. *Publ. Astron. Soc. Jpn.* 70(6):103
- Treumann RA. 2006. *Astron. Astrophys. Rev.* 13:229–315
- Tuntsov AV. 2014. *MNRAS* 441:L26–30
- van Waerbeke L, Zhitnitsky A. 2019. *Phys. Rev. D* 99:043535
- Vazza F, Brüggen M, Hinz PM, et al. 2018. *MNRAS* 480:3907–15
- Vedantham HK, Ravi V, Hallinan G, Shannon RM. 2016a. *Ap. J.* 830:75
- Vedantham HK, Ravi V, Mooley K, et al. 2016b. *Ap. J. Lett.* 824:L9
- Vergani SD, Salvaterra R, Japelj J, et al. 2015. *Astron. Astrophys.* 581:A102
- Voit GM, Evrard AE, Bryan GL. 2001. *Ap. J. Lett.* 548:L123–26
- Vorgul I, Kellett BJ, Cairns RA, et al. 2011. *Phys. Plasmas* 18:056501
- Wang C, Lai D, Han J. 2010. *MNRAS* 403:569–88
- Wang YK, Wang FY. 2018. *Astron. Astrophys.* 614:A50
- Waxman E. 2017. *Ap. J.* 842:34
- Weber J. 1970. *Phys. Rev. Lett.* 25:180–84
- Williams PKG, Berger E. 2016. *Ap. J. Lett.* 821:L22
- Wolszczan A, Cordes JM. 1987. *Ap. J. Lett.* 320:L35–39
- Wu XF, Zhang SB, Gao H, et al. 2016. *Ap. J. Lett.* 822:L15
- Xu S, Zhang B. 2016. *Ap. J.* 832:199
- Yamasaki S, Totani T, Kiuchi K. 2018. *Publ. Astron. Soc. Jpn.* 70:39
- Yang YP, Luo R, Li Z, Zhang B. 2017. *Ap. J. Lett.* 839:L25
- Yao JM, Manchester RN, Wang N. 2017. *Ap. J.* 835:29
- Yu YW, Cheng KS, Shiu G, Tye H. 2014. *J. Cosmol. Astropart. Phys.* 11:040
- Zhang B. 2017. *Ap. J. Lett.* 836:L32
- Zhang B. 2018. *Ap. J. Lett.* 854:L21
- Zhang YG, Gajjar V, Foster G, et al. 2018. *Ap. J.* 866(2):149
- Zheng Z, Ofek EO, Kulkarni SR, et al. 2014. *Ap. J.* 797:71
- Zhou B, Li X, Wang T, et al. 2014. *Phys. Rev. D* 89:107303

Contents

Nancy Grace Roman and the Dawn of Space Astronomy <i>Nancy Grace Roman</i>	1
Angular Momentum Transport in Stellar Interiors <i>Conny Aerts, Stéphane Mathis, and Tamara M. Rogers</i>	35
Millimeterwave and Submillimeterwave Laboratory Spectroscopy in Support of Observational Astronomy <i>Susanna L. Widicus Weaver</i>	79
Cometary Chemistry and the Origin of Icy Solar System Bodies: The View After Rosetta <i>Kathrin Altwegg, Hans Balsiger, and Stephen A. Fuselier</i>	113
The Properties of the Solar Corona and Its Connection to the Solar Wind <i>Steven R. Cranmer and Amy R. Winebarger</i>	157
New View of the Solar Chromosphere <i>Mats Carlsson, Bart De Pontieu, and Viggo H. Hansteen</i>	189
Star Clusters Across Cosmic Time <i>Mark R. Krumholz, Christopher F. McKee, and Joss Bland-Hawthorn</i>	227
The Most Luminous Supernovae <i>Avishay Gal-Yam</i>	305
Cosmological Tests of Gravity <i>Pedro G. Ferreira</i>	335
The Faintest Dwarf Galaxies <i>Joshua D. Simon</i>	375
Fast Radio Bursts: An Extragalactic Enigma <i>James M. Cordes and Shami Chatterjee</i>	417
Relativistic Jets from Active Galactic Nuclei <i>Roger Blandford, David Meier, and Anthony Readhead</i>	467
Understanding Galaxy Evolution Through Emission Lines <i>Lisa J. Kewley, David C. Nicholls, and Ralph S. Sutherland</i>	511

Accuracy and Precision of Industrial Stellar Abundances <i>Paula Jofré, Ulrike Heiter, and Caroline Soubiran</i>	571
Exoplanetary Atmospheres: Key Insights, Challenges, and Prospects <i>Nikku Madhusudhan</i>	617

Indexes

Cumulative Index of Contributing Authors, Volumes 46–57	665
Cumulative Index of Article Titles, Volumes 46–57	668

Errata

An online log of corrections to *Annual Review of Astronomy and Astrophysics* articles may be found at <http://www.annualreviews.org/errata/astro>